ARMY RESEARCH LABORATORY

Effects of Plasma Injection Duration and Position on Solid Propellant Electrothermal Gun Performance

A. E. Wildegger-Gaissmaier
G. P. Wren
A. Hosangadi

ARL-TR-994 April 1996

NOTICES

Destroy this report when it is no longer needed. DO NOT return it to the originator.

Additional copies of this report may be obtained from the National Technical Information Service, U.S. Department of Commerce, 5285 Port Royal Road, Springfield, VA 22161.

The findings of this report are not to be construed as an official Department of the Army position, unless so designated by other authorized documents.

The use of trade names or manufacturers' names in this report does not constitute indorsement of any commercial product.

DISCLAIMER NOTICE

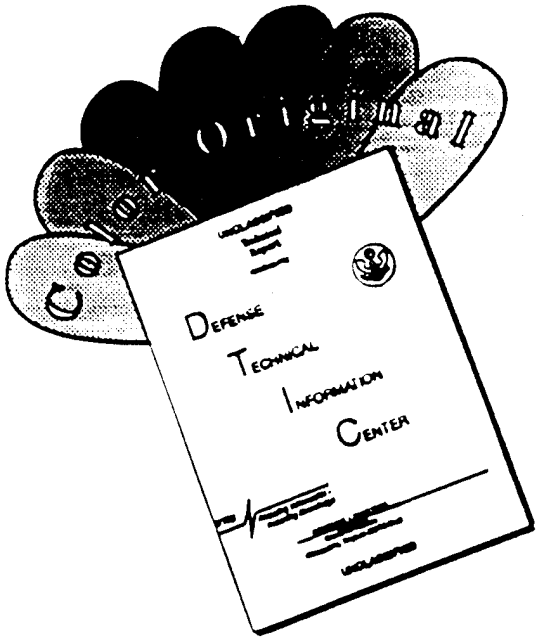

THIS DOCUMENT IS BEST QUALITY AVAILABLE. THE COPY FURNISHED TO DTIC CONTAINED A SIGNIFICANT NUMBER OF COLOR PAGES WHICH DO NOT REPRODUCE LEGIBLY ON BLACK AND WHITE MICROFICHE.

REPORT DOCUMENTATION PAGE

Form Approved
OMB No. 0704-0188

1. AGENCY USE ONLY *(Leave blank)*	2. REPORT DATE	3. REPORT TYPE AND DATES COVERED
	April 1996	Final, Oct 94 - Jun 95

4. TITLE AND SUBTITLE
Effects of Plasma Injection Duration and Position on Solid Propellant Electrothermal Gun Performance

5. FUNDING NUMBERS
PR: 1L162618A1FL

6. AUTHOR(S)
A. E. Wildegger-Gaissmaier, G. P. Wren, and A. Hosangadi

7. PERFORMING ORGANIZATION NAME(S) AND ADDRESS(ES)
U.S. Army Research Laboratory
ATTN: AMSRL-WT-PA
Aberdeen Proving Ground, MD 21005-5066

8. PERFORMING ORGANIZATION REPORT NUMBER
ARL-TR-994

9. SPONSORING/MONITORING AGENCY NAMES(S) AND ADDRESS(ES)

10.SPONSORING/MONITORING AGENCY REPORT NUMBER

11. SUPPLEMENTARY NOTES

12a. DISTRIBUTION/AVAILABILITY STATEMENT
Approved for public release; distribution is unlimited.

12b. DISTRIBUTION CODE

13. ABSTRACT *(Maximum 200 words)*

The performance of solid propellant electrothermal (SPETC) guns, besides being dependent on the total electrical energy used, is also influenced by the time frame and region over which the electrical energy is deposited. There is expected to be a point in the interior ballistic cycle where additional electrical energy input does not result in a significant projectile velocity increase since the electrically heated gases may not even reach the projectile. The aim of this study is to gain a clearer understanding of the plasma propellant interaction over the whole interior ballistic cycle and provide guidance to the selection of experimental parameters to optimize SPETC gun performance.

14. SUBJECT TERMS	15. NUMBER OF PAGES
electrothermal, interior ballistics	58
	16. PRICE CODE

17. SECURITY CLASSIFICATION OF REPORT	18. SECURITY CLASSIFICATION OF THIS PAGE	19. SECURITY CLASSIFICATION OF ABSTRACT	20. LIMITATION OF ABSTRACT
UNCLASSIFIED	UNCLASSIFIED	UNCLASSIFIED	UL

INTENTIONALLY LEFT BLANK.

TABLE OF CONTENTS

INTENTIONALLY LEFT BLANK.

LIST OF FIGURES

LIST OF TABLES

INTENTIONALLY LEFT BLANK.

1. INTRODUCTION

Electrothermal-chemical (ETC) guns utilize an electrically generated plasma formed by a pulsed power system in conjunction with a chemical propellant to increase the performance of the gun. The combustion process of solid propellants in an ETC system (SPETC) is initiated by the plasma, and the total energy is augmented by plasma injection into the gun chamber and/or in the barrel. The plasma/propellant combination can provide control of the combustion process in two ways: directly, by modifying the burning rate of the propellant, or indirectly, by influencing the space-mean pressure. An experimental investigation conducted by the North Carolina State University (Edwards, Bourham, and Gilligan 1995) showed a strong influence of the plasma on the burning rate of a propellant. Theoretical (Glick 1967) and experimental studies (Juhasz, Doali, and Bowman 1981) have also shown an influence of grain temperature on the burn rate of a propellant. The plasmas used in ETC applications have temperatures of about 10,000–30,000 K, and thus an initial grain temperature rise of the propellant through radiative heating is considered feasible (White et al. 1995). The burning rate of a solid propellant, besides being sensitive to grain temperature, is also dependent on the pressure. Injection of plasma can increase the duration of the high-pressure regime in the interior ballistic cycle, and, therefore, increase the effective mass generation rate per unit time of the propellant. This is of special importance for high loading density charges, which are often not totally burnt out at the end of the interior ballistic cycle when using conventional ignition stimuli. The beneficial influence of enhancing the combustion by plasma injection for high loading density charges has been shown by White et al. (1995).

The performance of SPETC guns, besides being dependent on the total electrical energy used, is also influenced by the time frame and region over which the electrical energy is deposited. There is expected to be a point in the interior ballistic cycle where additional electrical energy input does not result in a significant projectile velocity increase since the electrically heated gases may not even reach the projectile. The aim of this study is to gain a clearer understanding of the plasma propellant interaction over the whole interior ballistic cycle and provide guidance to the selection of experimental parameters to optimize SPETC gun performance.

A number of interior ballistic models with varying degrees of complexity have been developed to investigate the influence of plasma augmentation on the interior ballistic cycle. Zero-dimensional (0-D) codes assume instantaneous communication between the breech and the base of the projectile via a pressure-gradient relationship. The injection duration and region over which electrical energy is deposited

(as long as the projectile is in the barrel) does not influence the model predictions greatly. However, the total amount of electrical energy consumed is critical. One-dimensional (1-D) codes remove the pressure gradient assumption by solving the flow equations directly. Thus, the interior ballistic cycle is influenced by such factors as the duration and rate of addition of the electrical energy. However, as shown in previous studies (Wren et al. 1995), the spatial distribution of the plasma must be considered in the case of high electrical energy densities in order to provide good agreement with experimental data. Two-dimensional (2-D) codes allow both a radial and axial description of the plasma/propellant interactions.

This study is based on an experimental gun firing, and the 0-D and 1-D models are validated using the experimental data. The experimental case is then extended to consider the influence of the duration, rate of addition of electrical energy, and position of the plasma jets on gun performance. Efficiency of plasma addition to the gun is considered with the various modeling approaches.

2. MODEL DESCRIPTIONS

2.1 0-D Model. The lumped parameter model IBHVG2.ETC (Ernhart, Winsor, and Wren 1994) has been used for the 0-D case. Lumped parameter models include the major physical processes, treating the regions of the gun uniformly in regard to the physical properties. A Lagrange pressure gradient between the breech and base of the projectile is assumed, and communication is instantaneous. The model assumes that the plasma energy is a source term in the overall energy equation. The plasma properties based on experimental data or design parameters for the plasma injector are used as input parameters in each time step. The nature of the model implies a direct relationship between the chemical and electrical energy expended and the gun performance. The position (being a 0-D model) and duration of plasma injection (as long as the projectile is still in the barrel) have no influence on the performance predictions.

2.2 1-D Model. 1-D two-phase flow models allow a more accurate description of the interior ballistic process. The XNOVAKTC (XKTC) code has been developed by Paul Gough Associates (Gough 1983). For a detailed basic description of the code, the authors again refer to Gough (1983, 1979). The code is based on the 1-D, transient, heterogeneous two-phase flow equations. The balance equations for energy, mass, and momentum for the two phases are solved numerically using an explicit finite difference (McCormack predictor/corrector) scheme. The covolume equation of state of the gas phase supports the balance equations. A control volume approach computes average flow properties in a cell large in comparison to the size of propellant grains.

The complex processes between the boundary layers of the two phases are not modeled from first principles. Assumptions have been made that empirical correlations for interphase drag, heat transfer, and combustion rate adequately describe the physical processes. The propellant bed is contained between the gun breech face, gun chamber walls, and the base of the projectile, which are the external physical boundaries.

The plasma source represents a boundary condition and is incorporated as a source of mass, momentum, and energy in the gas-phase balance equations. The plasma is described using a plasma mass and energy flux which are added to the gas phase over a mixing length. One or multiple plasma sources can be modeled. The plasma jets are represented by a number of fixed regions where the jets are mixed and overlapping of the regions can be examined. The plasma is specified by experimental data or design parameters including the plasma energy, plasma mass flux over time, and a mixing length.

The decomposition of the propellant can be modeled using several laws: (1) the conventional burning rate law, where the burn rate is dependent on pressure; (2) a Hemholtz law using incremental specific data; and (3) a tabular specification of mass or linear rate. For the current investigation, the first option, pressure-dependent burning rate, was chosen.

2.3 2-D Model. It has been shown in previous studies (Wren et al. 1995) that the spatial distribution of the plasma plays an important role in the interior ballistic cycle of ETC guns, particularly when high electrical energy densities are involved. As already pointed out, the plasma influences the combustion behavior of the propellant. We assume, however, that the effect is confined to the area where the plasma penetrates the propellant bed and interacts directly with the propellant. To be able to estimate which propellant grains are in contact with the plasma, the code would have to keep track of the axial and radial position of single-propellant grains. Furthermore, a 1-D interior ballistics code is not able to handle any radial penetration of the plasma, and, in addition, only bulk properties of the propellant (e.g., average porosity in each computational cell) can be considered. This makes it important to apply a code which is able to track the position of single-propellant grains and to compute the radial penetration of the plasma.

The 2-D gun propulsion version of the CRAFT (Hosangadi, Sinha, and Dash 1994) code developed by Combustion, Research, and Flow Technology Inc., is based on first principles. The code solves reacting, multiphase, multicomponent fluid flow equations and allows the computation of the 2-D solid propellant interior ballistics flow fields. The two-phase flow is described as a mixture of continuum fluid

(which can be liquid, gas, or a combination of liquid and gas) and an aggregate of incompressible particles. The gas phase equations for dense two-phase flows are similar to those used in the 1-D XKTC (Gough 1979) code. A Lagrangian formulation describes the motion of the propellant grains where each grain is tracked independently in terms of dimension, motion, and gas generation rate. Similar empirical relations used in the 1-D code are utilized for drag and heat transfer to model the processes occurring between the solid propellant grain and the gas surrounding it. Nonequilibrium between the two phases as well as phase change for the particles as they heat up or cool down are considered. Combustion is modeled with the conventional pressure-dependent burning-rate law. The numerics used are an implicit higher order upwind (Roe/TVD) formulation with fully implicit source terms and boundary conditions.

The model is directly coupled with a plasma capillary model (Powell and Zielinski 1992). The plasma injection is subsonic for the major part of the injection period; therefore, the plasma properties are dependent on the pressure within the gun chamber. To be able to accurately compute the plasma properties, the plasma code has to be coupled with the CRAFT code. The plasma code is 1-D, quasi-steady, and isothermal (Kaplan et al. 1995). The velocity, temperature, and pressure (if chocked) computed by the plasma code represent the injection conditions for the CRAFT code. The CRAFT code computes the pressure at the coupling plane and specifies the boundary condition to the plasma code. The input parameters for the plasma are specified by experimental data or design parameters and include, along with the dimensions of the capillary, the current-time history. The current version of the code permits only breech-injected plasmas.

3. MODEL VALIDATION

An experimental gun firing* (Kaplan et al. 1995) was chosen to validate the 0-D and 1-D models. The experimental parameters are listed in Table 1. The total electrical energy expended during the experiment was 1.463 MJ, and the charge weight was 6.3 kg. Figure 1 shows the experimental pressure time curve and model predictions for IBHVG2 and XKTC models. Table 2 lists the maximum pressures and muzzle velocities. As one can see, even though the pressure-time curves are not identical, reasonable agreement between experimental data and model predictions was achieved for maximum pressure and muzzle velocity for IBHVG2. The XKTC model predicted a 4.3% lower maximum pressure and a 1.1% higher muzzle velocity. The charge weight of 6.3 kg represents a loading density of 0.94 g/cm^3.

* Data supplied by Soreq Nuclear Research Center, Yarne, Israel.

Table 1. Experimental Parameters

Parameter	Description
Caliber	105 mm
Chamber Volume	0.006704 m^3
Propellant	M30
Charge Weight	6.30 kg
Grain Form	19 hexagonal

The 1-D version of the CRAFT code was validated earlier against the 1-D XKTC code (Powell and Zielinski 1992). The earlier validation was based on a spherical propellant grain. For the prevailing case, a 19-hexagonal form function was included in the code and comparisons made with XKTC model predictions. Figures 2a–2d show pressure and temperature profiles for XKTC and 1-D CRAFT simulations in the case of a closed-bomb firing, assuming no losses. For this case, an analytical solution exists. In all closed-bomb cases investigated, the CRAFT code obtained the analytical solution in regard to maximum pressure and temperature. As can be seen, the results of XKTC and CRAFT are identical for spherical propellant grains. For the 19-hexagonal grain, the XKTC model predicts a lower maximum pressure compared to CRAFT. This can be attributed to the nonconservative nature of the XKTC code, where mass and energy are not preserved. The mass defects for the XKTC model predictions were –1.53% for the 19-hexagonal grain and –0.01% for the spherical grain. Figure 3 shows the results of a gun simulation (1-D case) for a 0.75-g/cm^3 loading density comparing pressure-time histories predicted by CRAFT and XKTC. The agreement between the two models is good, considering the nonconservative nature of the XKTC code.

4. PARAMETRIC STUDY

A parametric study was conducted to extend the experimental case. The IBHVG2 and XKTC models described previously were utilized for the investigation. A number of parameters were considered, including the injection duration, injection region, number of injection ports, and total amount of electrical energy consumed. The gun dimensions, charge weight, and projectile weight were identical to the model validation cases.

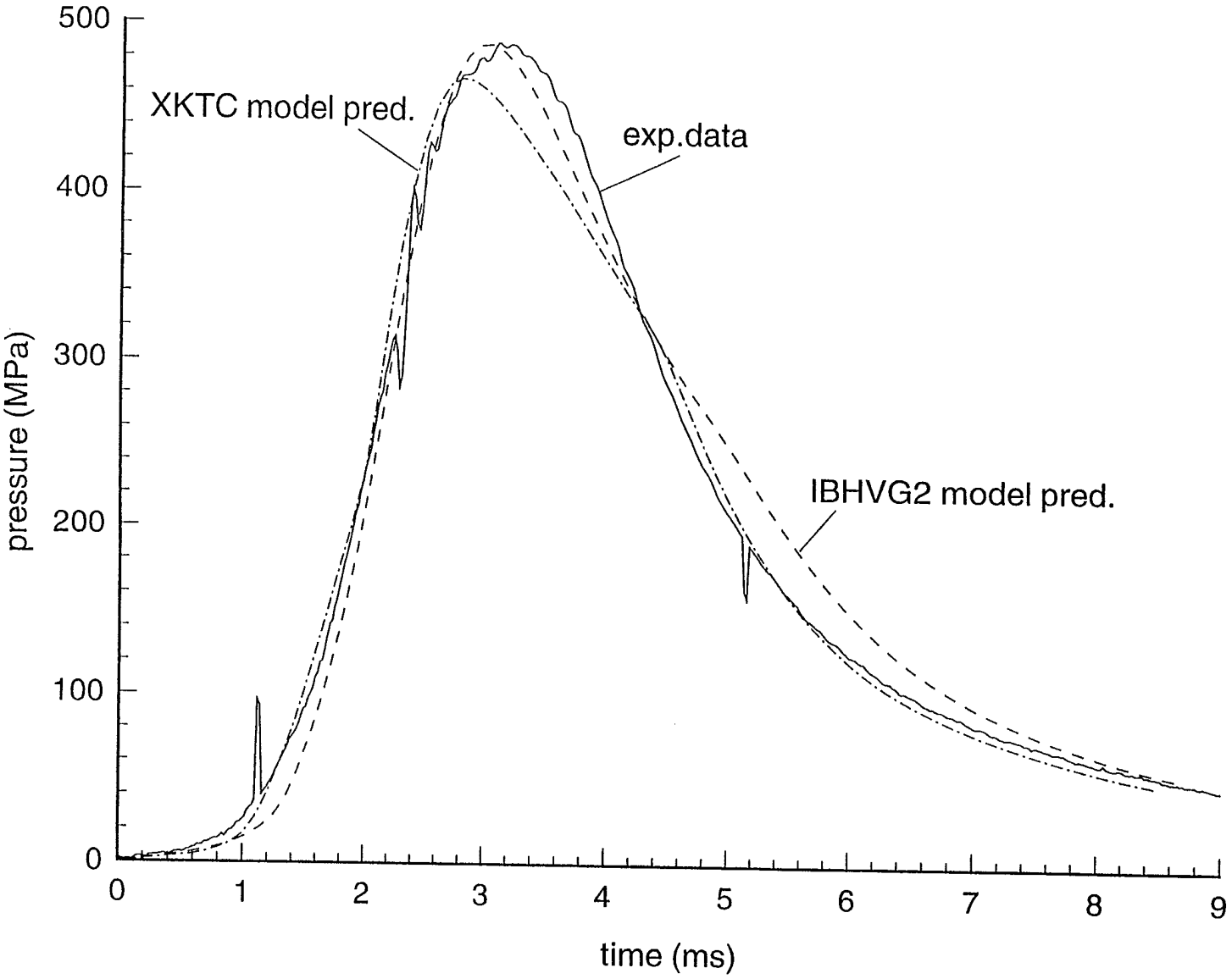

Figure 1. Comparison of experimental data and model predictions.

Table 2. Comparison of Experimental Data and Model Predictions

Characteristic	Experimental Data	IBHVG2	XKTC
Maximum Breech Pressure (MPa)	488	487.7	467.9
Muzzle Velocity (m/s)	2,003	1,994.8	2,025.7

4.1 Influence of Injection Duration on Performance. For the first part of the study, a square electrical pulse shape was assumed with a constant electrical power level, the parameter was varied with the duration of the pulse, and the total electrical energy input was dependent on the total injection time. The simulations were conducted for four different power levels (125-, 250-, 500-, and 750-MW power). Figures 4 and 5a show the muzzle velocities vs. injection times for the different power levels for IBHVG2 and XKTC model predictions, respectively. As one would expect, the muzzle velocity increases with injection duration for the IBHG2 model predictions (Figure 4). This is consistent with the assumption of the lumped parameter model, which infers an instantaneous communication between the breech and the base of the projectile via a pressure gradient relationship. Therefore, only the total plasma energy injected into the chamber is important. The relationship between amount of plasma energy injected and increase in projectile kinetic energy is not linear. The reasons are increasing heat loss and higher combustion gas exit temperatures and pressures with increasing electrical energy input.

The XKTC simulations were conducted assuming a breech-injected plasma with a mixing length of 0.57 m (length of the gun chamber). No experimental data are available to estimate the mixing length of the plasma jet, and the value was chosen to be consistent with the length of the combustion chamber. It can be observed in Figure 5a that the muzzle velocity for the same electrical energy input increases with increasing power levels. This would infer that a performance gain can be obtained by using higher electrical power pulses for the same amount of electrical energy. Figure 5b shows the muzzle velocities vs. injection times for the different power levels for XKTC model predictions. As can be seen in Figure 5b, in which the total amount of electrical energy varies with power and injection time, the XKTC model predicts an increase in muzzle velocity for injection durations up to approximately 4 ms for all power levels; after that time, the muzzle velocity stays constant. This implies that the electrical energy of the plasma is not translated into an increased projectile energy after some time. This is confirmed by Figure 6a–6d. The plots depict temperature contours in the gun from the breech to the projectile base in the interior ballistic cycle, position vs. time, for three injection durations (1, 4, and 6 ms). The high

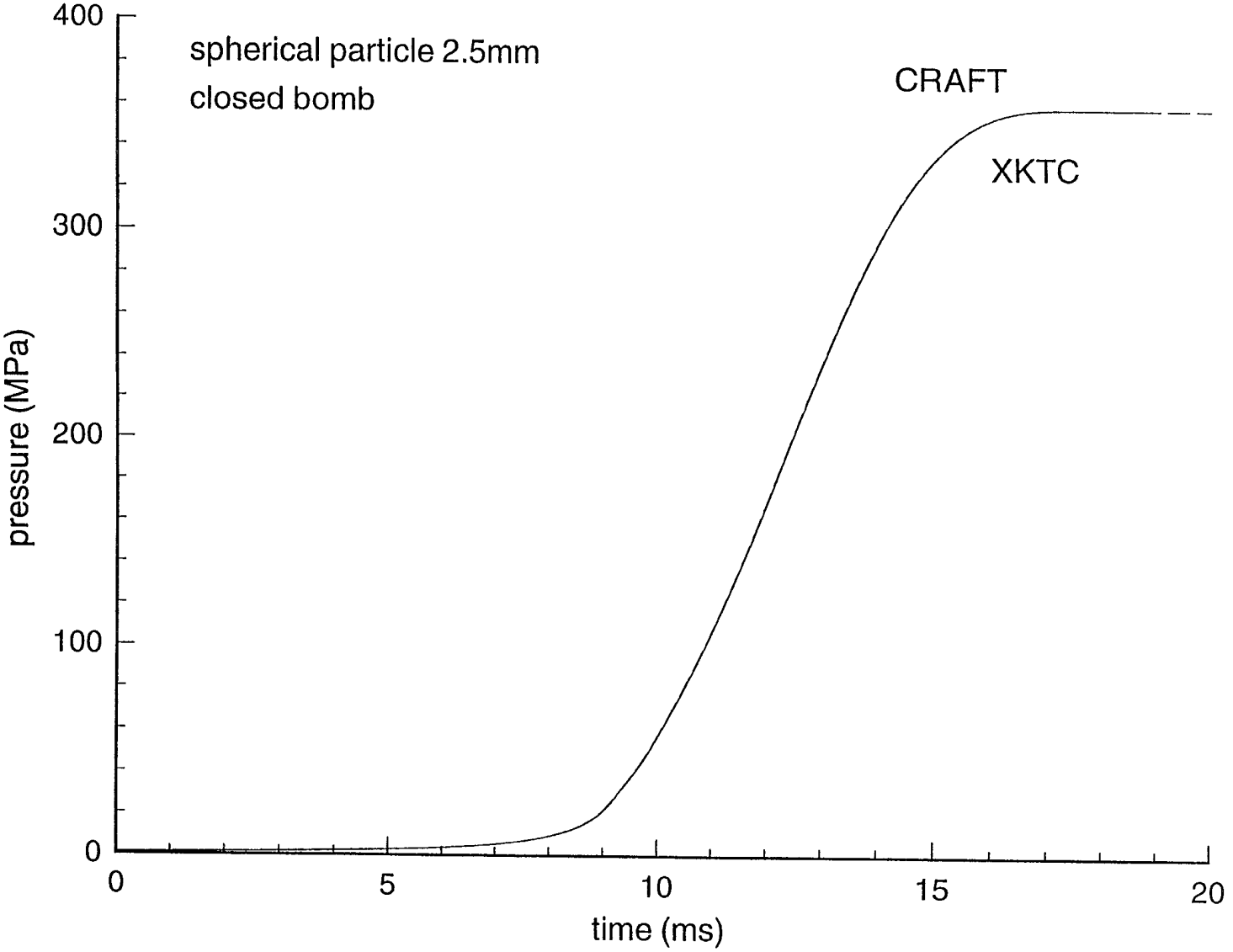

Figure 2a. Comparison of XKTC and CRAFT model predictions for pressure-time history 2.5-mm particles in closed bomb.

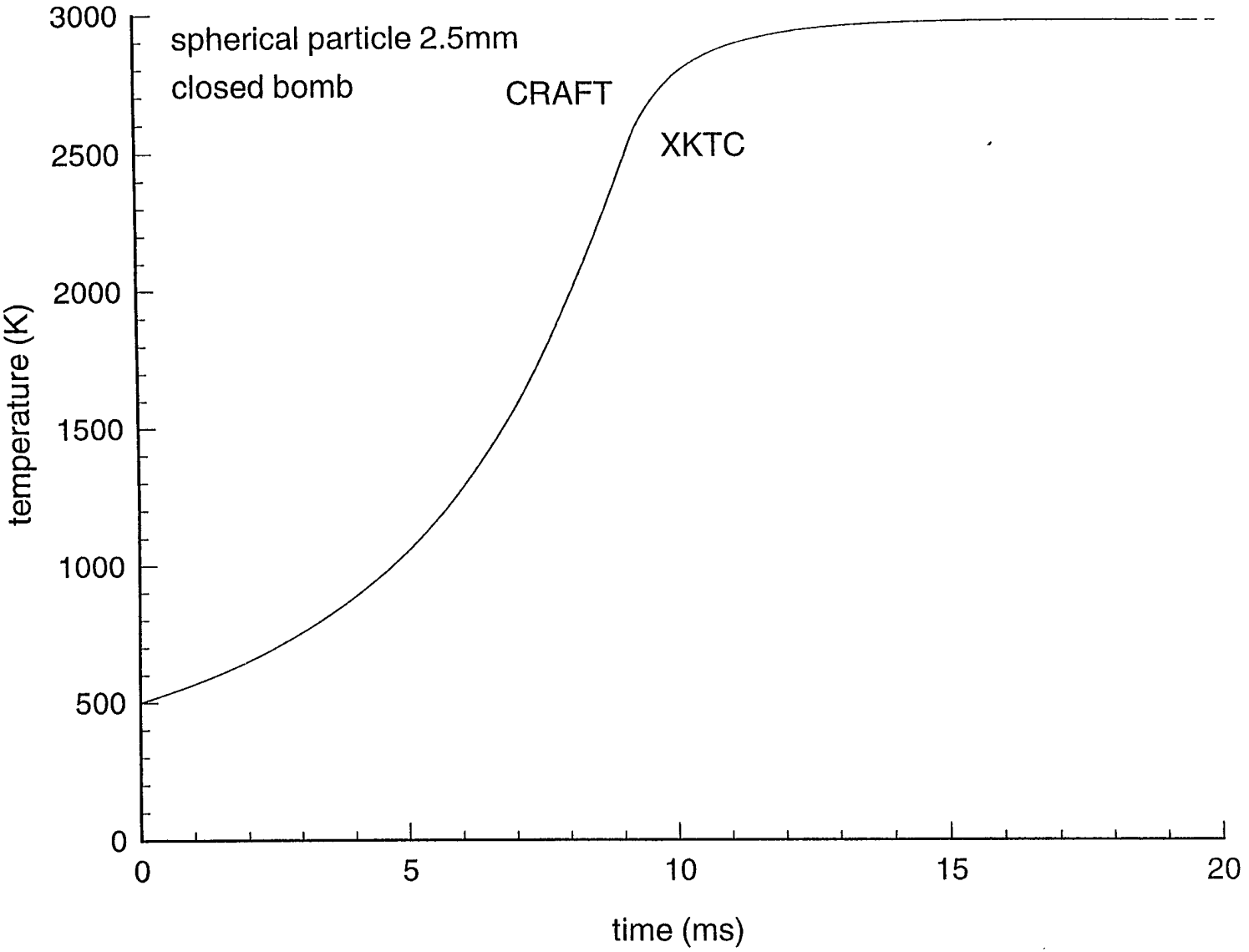

Figure 2b. Comparison of XKTC and CRAFT model predictions for temperature-time history 2.5-mm particles in closed bomb.

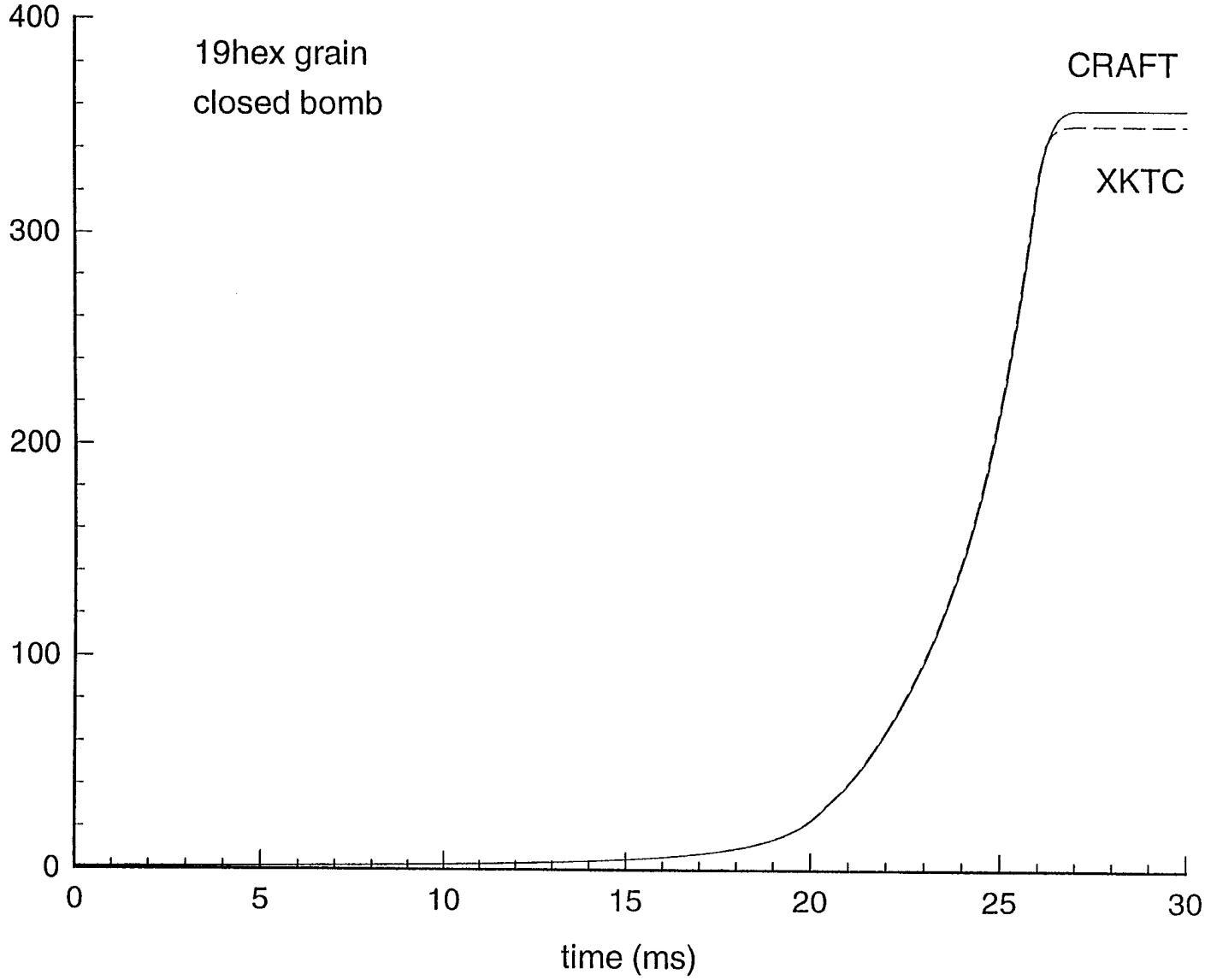

Figure 2c. Comparison of XKTC and CRAFT model predictions for pressure-time history 19-hex particles in closed bomb.

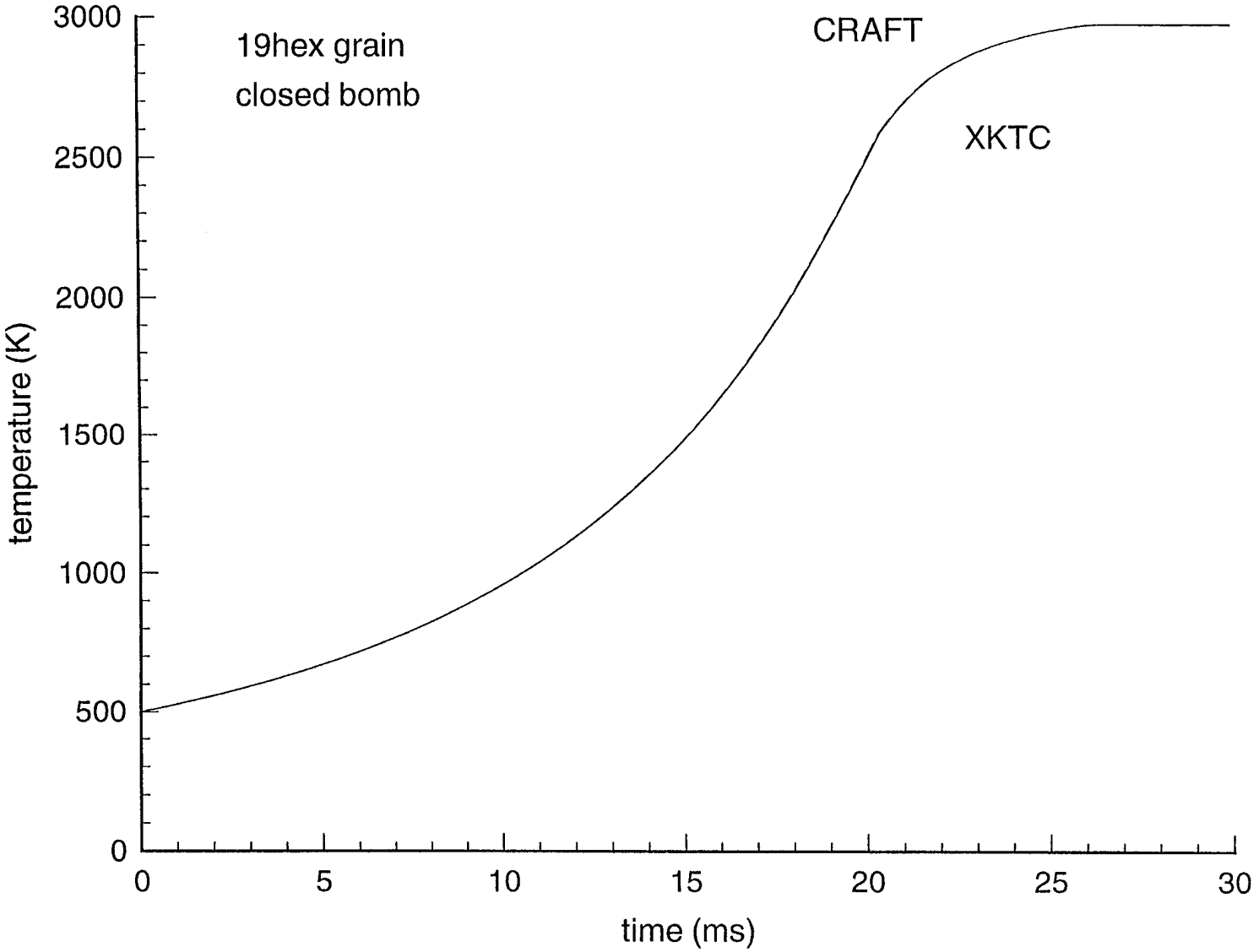

Figure 2d. Comparison of XKTC and CRAFT model predictions for temperature-time history 19-hex particles in closed bomb.

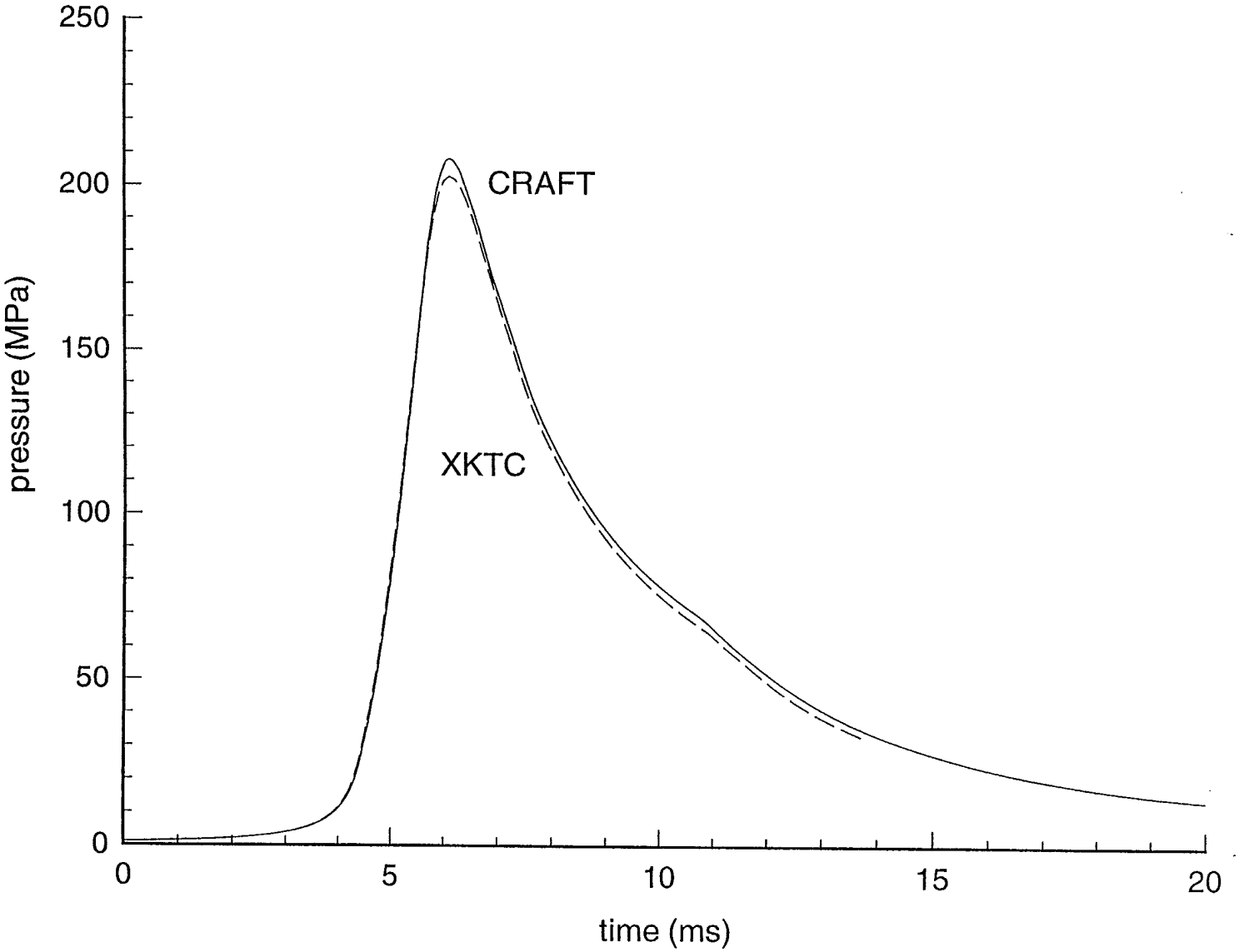

Figure 3. Comparison of XKTC and CRAFT model predictions for pressure-time history 19-hex grain, gun firing with loading density 0.75.

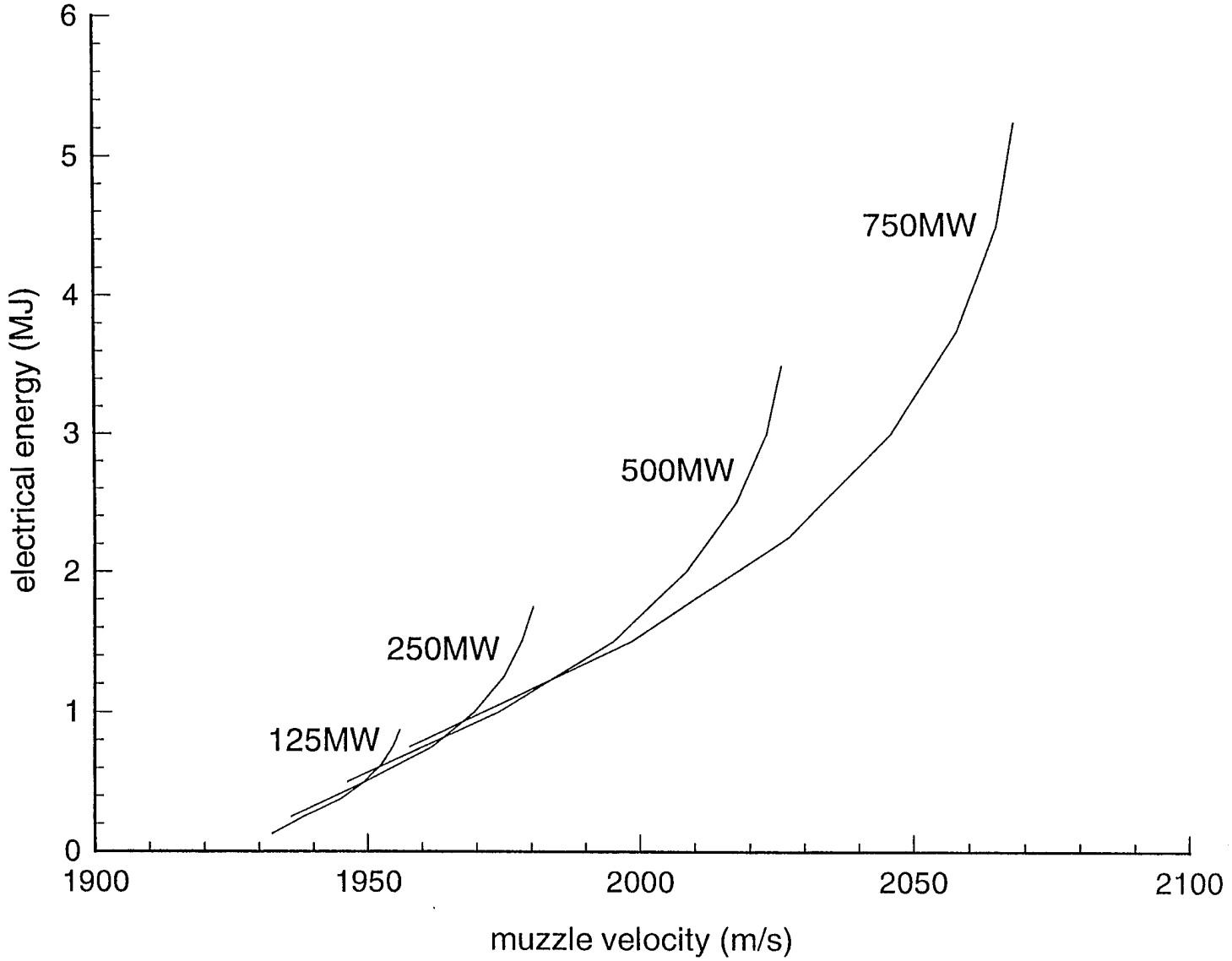

Figure 4. IBHVG2 model predictions: influence of electrical energy input on muzzle velocity.

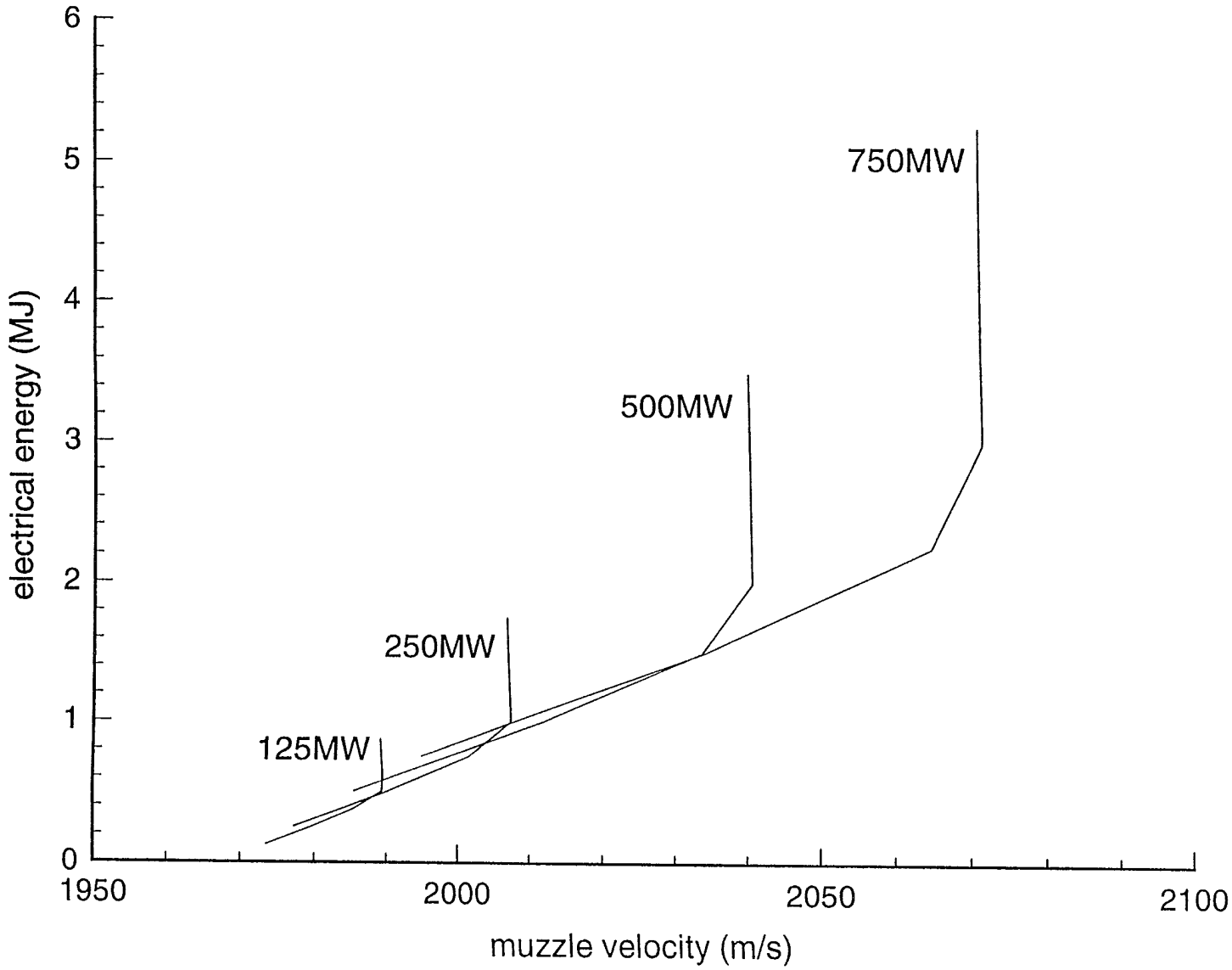

Figure 5a. XKTC model predictions: influence of electrical energy input on muzzle velocity.

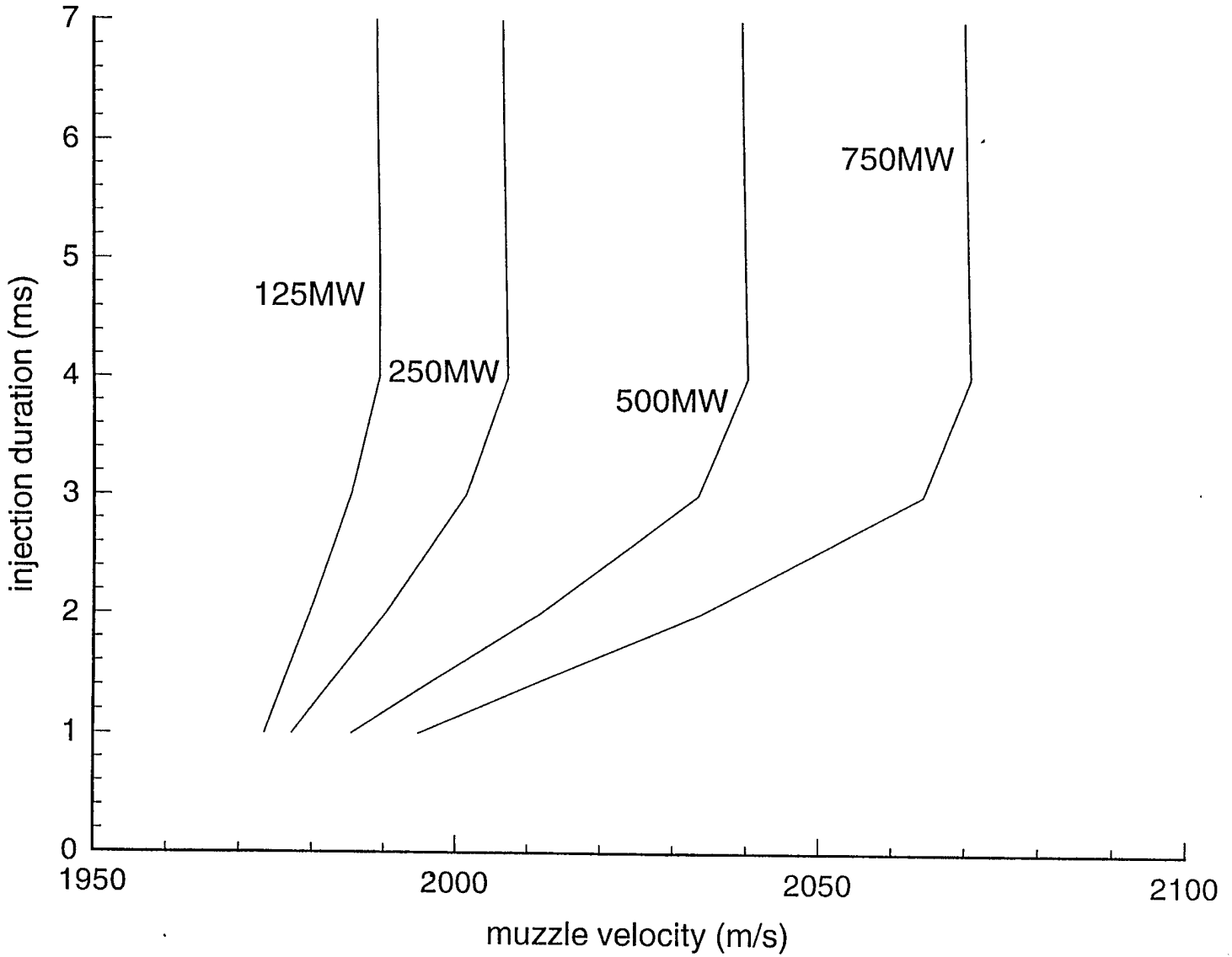

Figure 5b. XKTC model predictions: influence of injection duration on muzzle velocity.

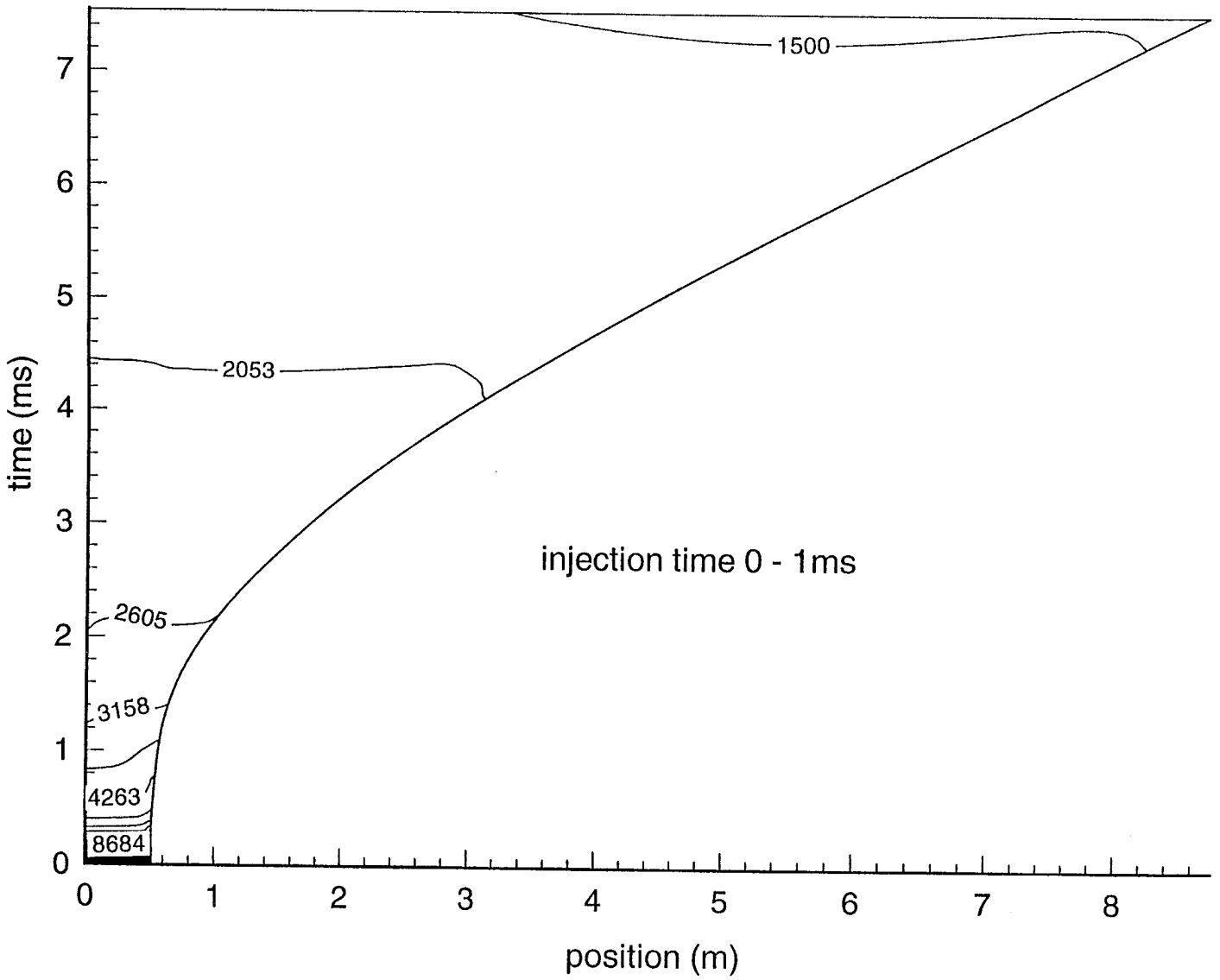

Figure 6a. Temperature contours for 1-ms plasma injection duration.

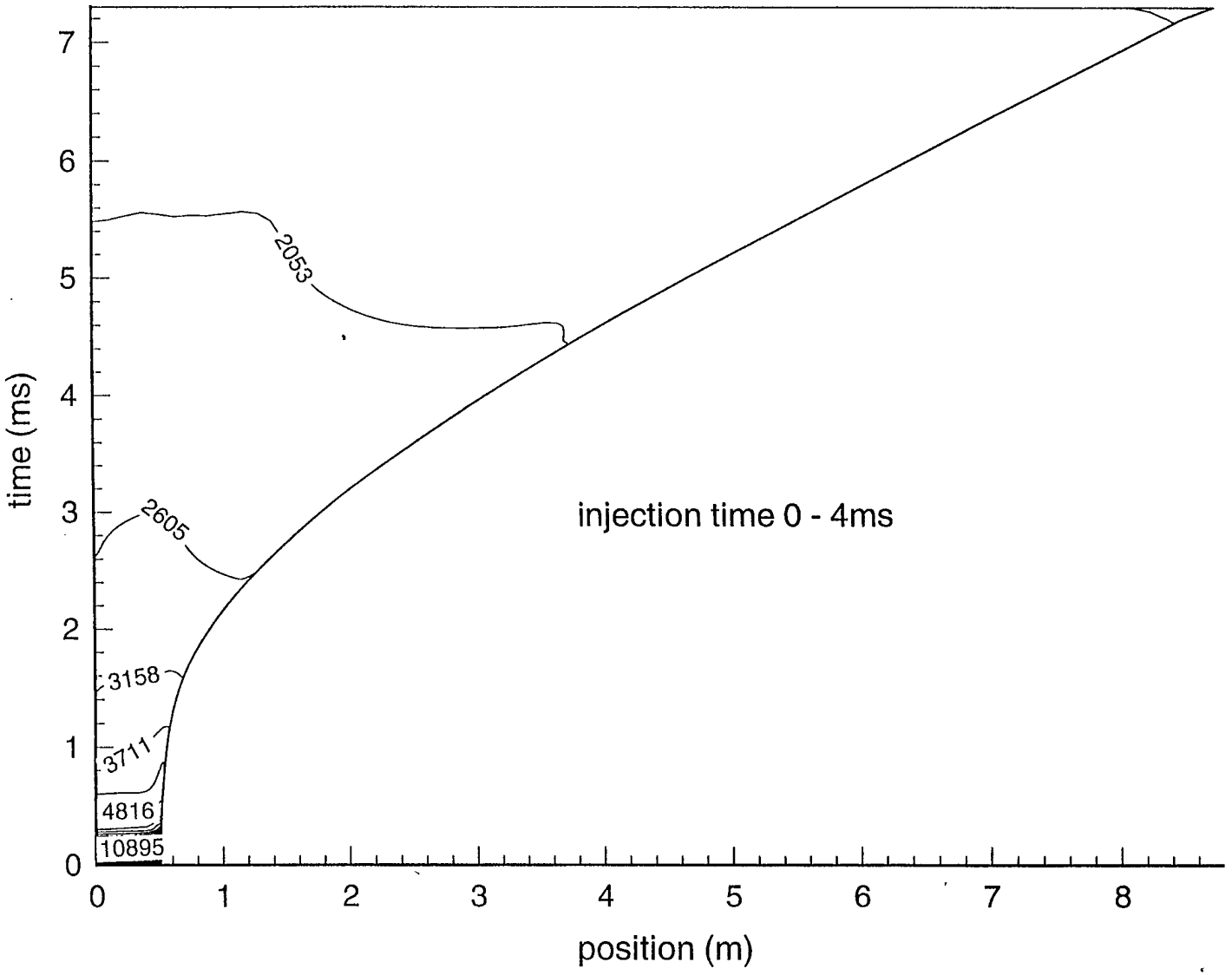

Figure 6b. Temperature contours for 4-ms plasma injection duration.

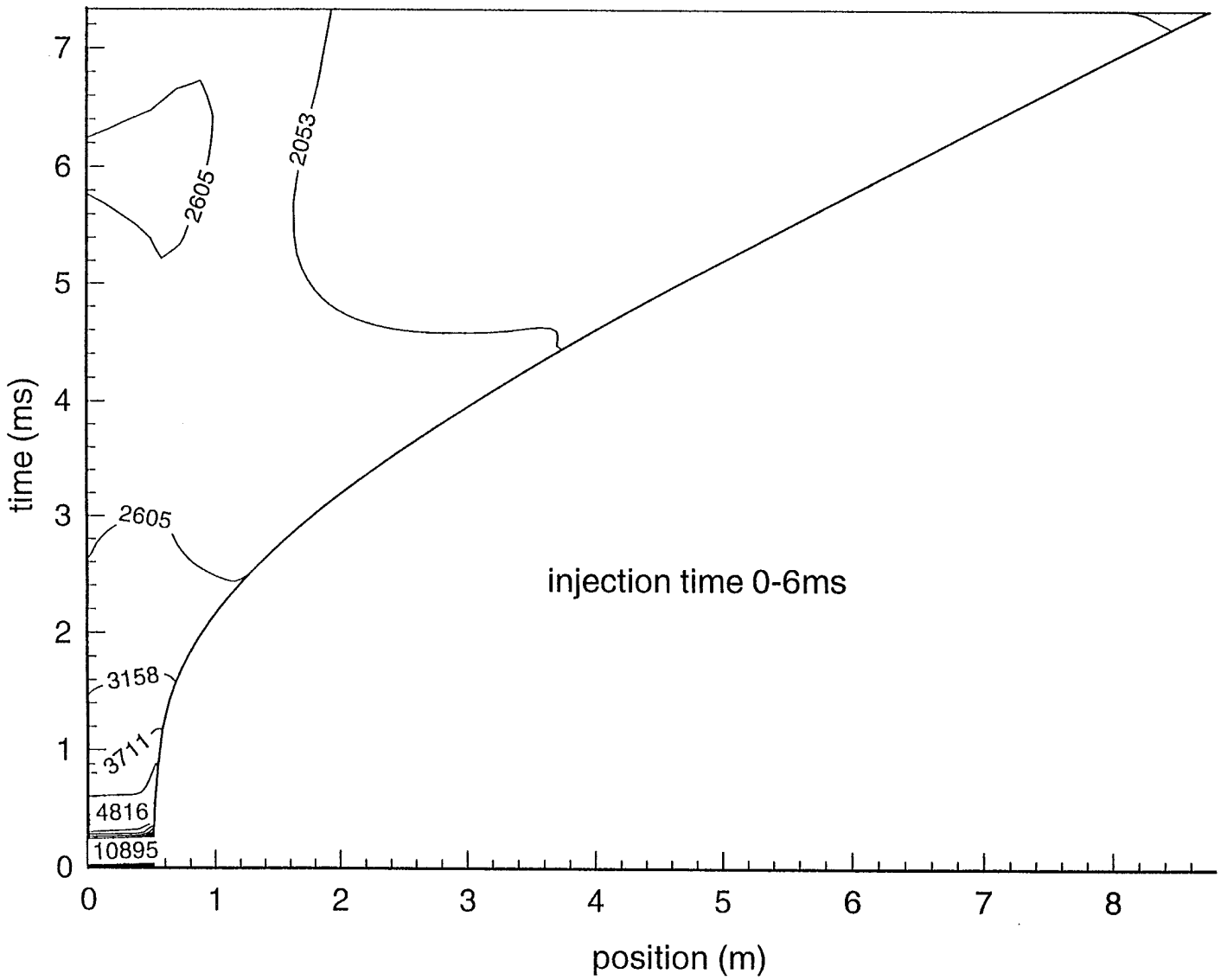

Figure 6c. Temperature contours for 6-ms plasma injection duration.

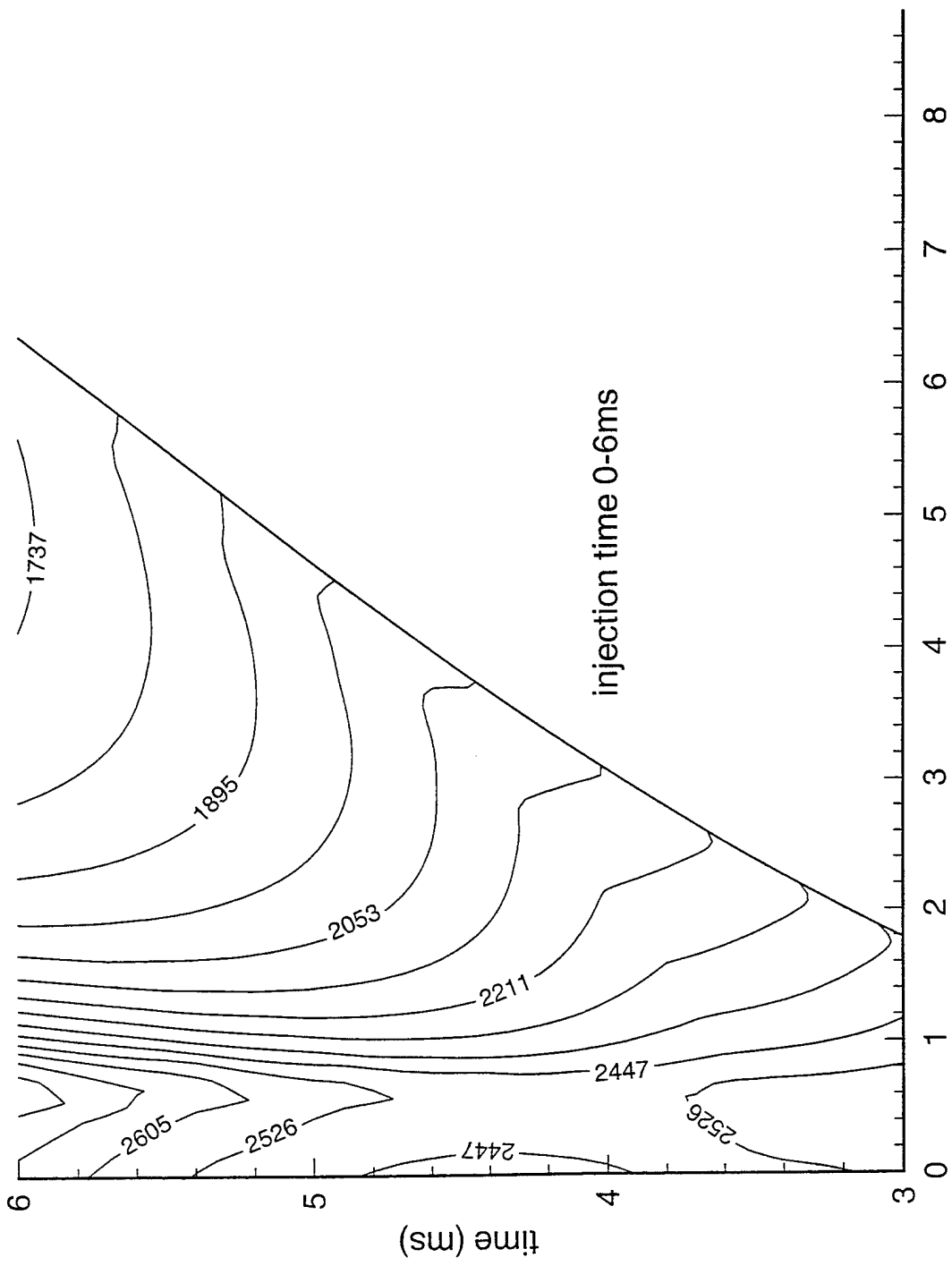

Figure 6d. Detailed temperature contours for 6-ms plasma injection duration.

temperature associated with the presence of the plasma and its heating of surrounding gases extends only to a limited region of the position-time curves in the plots. As one can see, the gas temperatures stay above 2,000 K up to approximately 4 ms. Additional plasma injection from 4–6 ms (Figure 6c) has an effect on gas temperatures only in the area near the breech. Due to the large temperature region involved in the plots (1,500–12,000 K), details of the gradient between the temperature contours are shown in Figure 6d for the time frame from 3–6 ms (temperature region 1,500–3,000 K). As can be seen, the temperature cools gradually from breech to projectile base.

XKTC simulations that varied the power level and kept the total energy constant show similar results. The plasma injection occurred again at the breech with a mixing length of 0.57 mm. Figure 7a shows the dependence of muzzle velocity on power level for five total energy levels. Again, as one can see, there is also a cutoff point where an increase in power does not result in any additional performance gain. At high power levels, a small decrease in muzzle velocity occurs, which is due to the increased heat loss with increasing electrical energy input. In Figure 7b, an electrical efficiency vs. electrical energy input has been depicted. The electrical efficiency is computed using the following expression:

$$\frac{KE_{tot} - KE_0}{EE} = e_{eff},$$

where KE_{tot} is the total kinetic energy of the projectile, KE_0 is the projectile kinetic energy derived from simulation without any electrical energy, and e_{eff} is the electrical energy efficiency factor. As can be seen, there is a point for each power level where losses are minimized and the electrical energy input is used most efficiently.

4.2 Influence of Injection Region on Performance. The previous simulations would suggest that injecting the electrical energy at different positions along the gun barrel to extend the high-temperature regime of the gases at the projectile base could be beneficial. Table 3 shows some examples where a number of injection points were utilized along the barrel. These examples are by no means an optimization; however, they give an indication of the performance improvements feasible when a number of plasma jets along the gun barrel are utilized. To obtain the optimum performance, one should time the plasma injections with the arrival of the projectile base at the plasma port. For the listed cases, the injection time itself was not optimized to coincide totally with the position of the projectile base. All of the simulations listed in Table 3 have been conducted with the 1-D model XKTC.

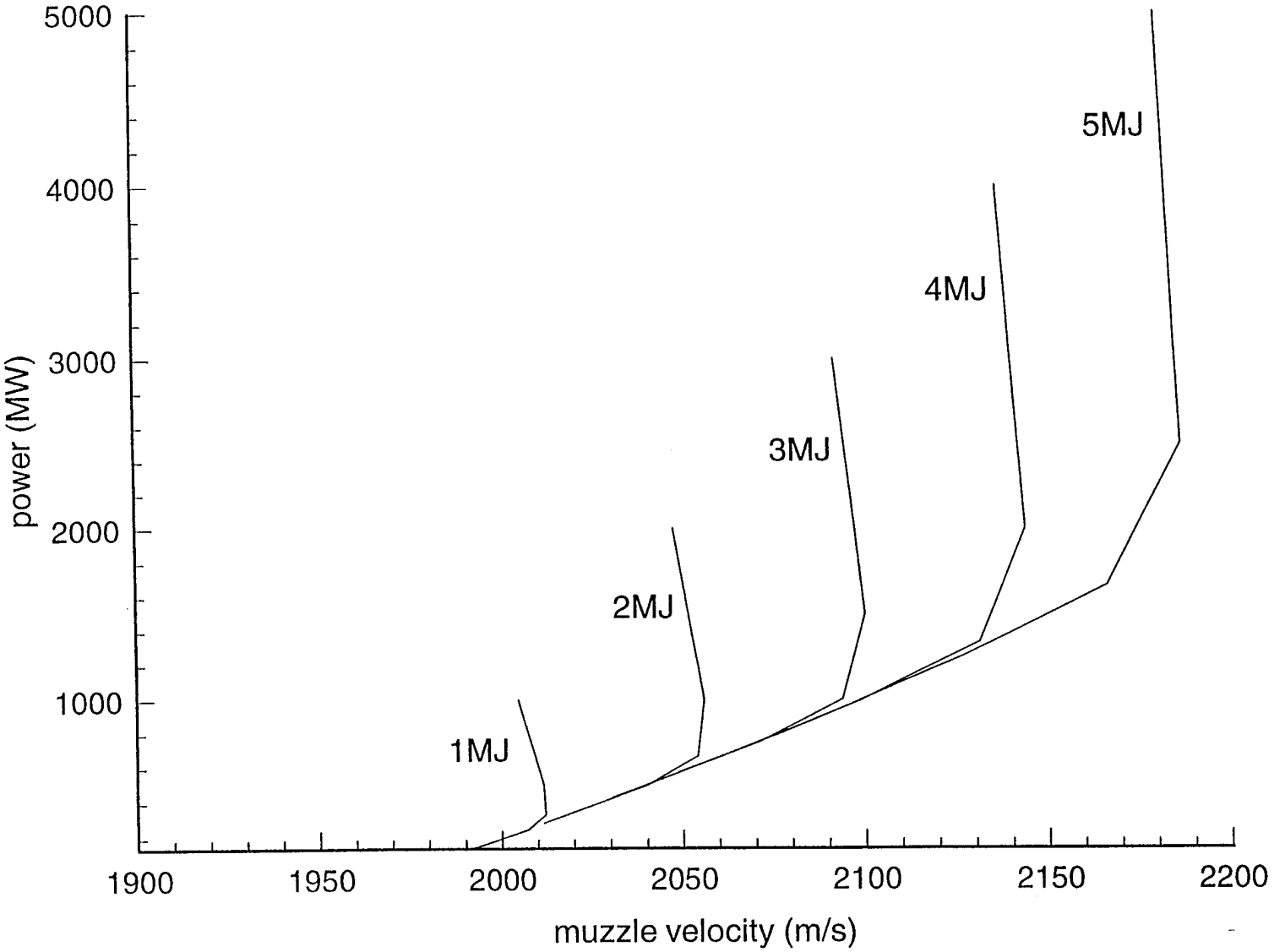

Figure 7a. Influence of power on muzzle velocity.

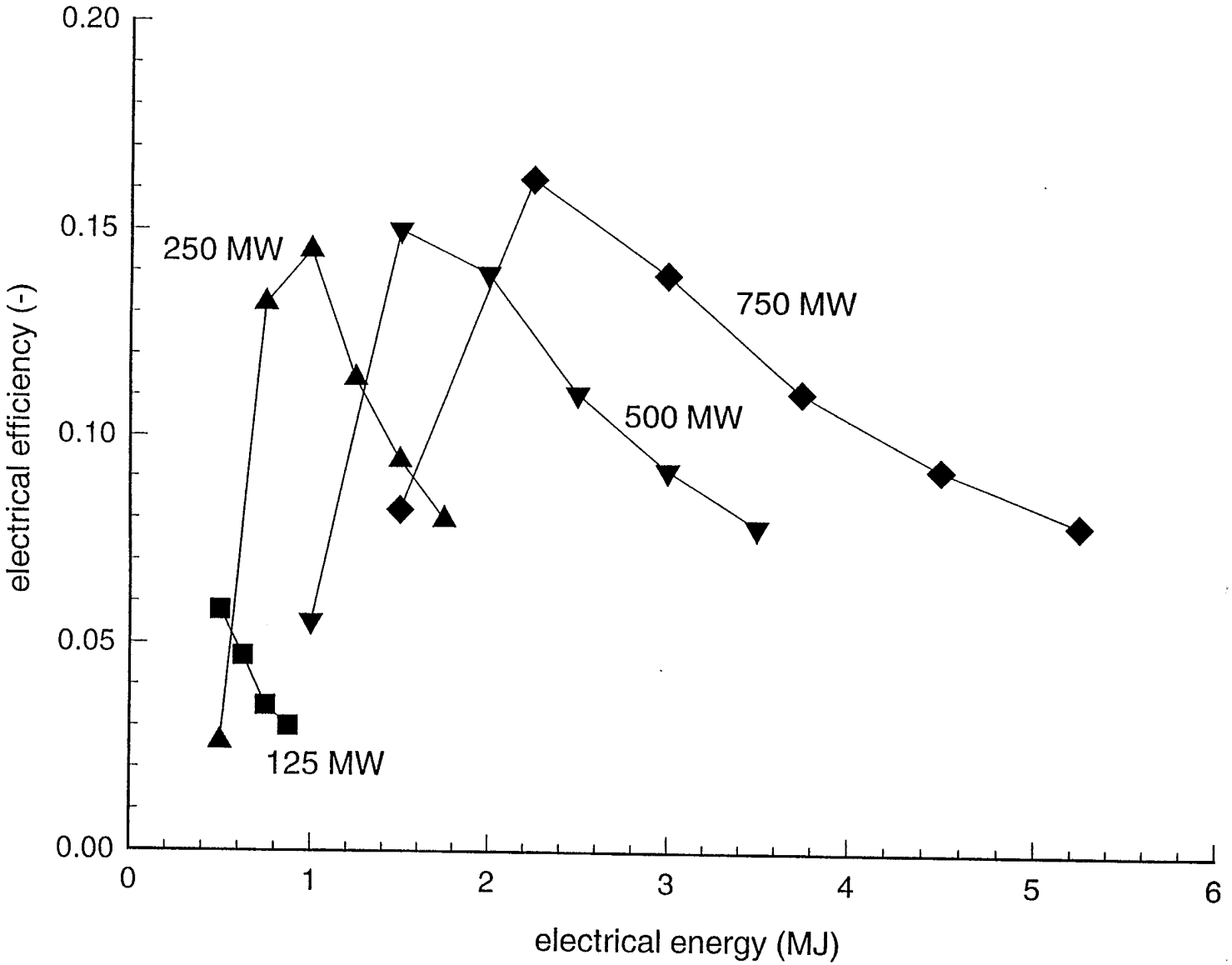

Figure 7b. Influence of power on electrical efficiency.

Table 3. Influence of Injection Region on Muzzle Velocity and Maximum Pressure

Case No. (–)	Jet (–)	Position From Breech (m)	Mixing Length (m)	Duration (ms)	Muzzle Velocity (m/s)	Maximum Pressure (MPa)	Electrical Energy (MJ)	Total Electrical Energy (MJ)
1	1	0.00	0.57	0–7	2,066.07	503.34	5.000	5.000
2	1	0.00	0.57	0–3.5	—	—	2.500	—
	2	2.00	0.50	3.5–7.0	—	—	2.500	—
	1–2	—	—	0–7	2,090.71	503.34	—	5.000
3	1	0.00	0.57	0–1.75	—	—	1.250	—
	2	0.25	0.50	1.75–3.5	—	—	1.250	—
	3	2.00	0.50	3.5–5.25	—	—	1.250	—
	4	4.90	0.50	5.25–7	—	—	1.250	—
	1–4	—	—	0–7	2,016.51	501.79	—	5.000
4	1	0.00	0.57	0–1	—	—	0.714	—
	2	0.20	0.50	1–2	—	—	0.714	—
	3	0.40	0.50	2–3	—	—	0.714	—
	4	1.40	0.50	3–4	—	—	0.714	—
	5	2.80	0.50	4–5	—	—	0.714	—
	6	4.50	0.50	5–6	—	—	0.714	—
	7	6.40	0.50	6–7	—	—	0.714	—
	1–7	—	—	0–7	2,132.04	505.45	—	5.000
5	1	0.00	0.57	0–1	—	—	0.3571	—
	2	0.20	0.50	1–2	—	—	0.3571	—
	3	0.40	0.50	1–2	—	—	0.3571	—
	4	1.40	0.50	3–4	—	—	0.3571	—
	5	2.80	0.50	4–5	—	—	0.3571	—
	6	4.50	0.50	5–6	—	—	0.3571	—
	7	6.40	0.50	6–7	—	—	0.3571	—
	1–7	—	—	0–7	2,072.54	474.30	—	2.500
6	1	0.00	0.57	0–1	—	—	0.3571	—
	2	0.20	0.50	1–2	—	—	0.3571	—
	3	0.40	0.50	2–3	—	—	0.3571	—
	4	1.40	0.50	3–4	—	—	0.3571	—
	5	2.80	0.50	4–5	—	—	0.714	—
	6	4.50	0.50	5–6	—	—	1.428	—
	7	6.40	0.50	6–7	—	—	1.428	—
	1–7	—	—	0–7	2,158.20	474.3	—	5.00

Case 1 in Table 3 shows the muzzle velocity and pressure prediction for a 5.0-MJ shot, a breech-injected plasma, a mixing length of 0.57 m, and an injection time duration of 7 ms. The power level is 714.3 MW. This case is used as a baseline for comparison with the following computations. In Case 4, the plasma is injected utilizing seven plasma ports along the gun barrel, the electrical energy is 0.714 MJ, and the injection duration is 1 ms, starting at different initial times for each jet. An improvement of 66 m/s in muzzle velocity (with approximately the same maximum pressure) compared to Case 1 was obtained. Case 4 is also depicted in Figure 8, where the temperature contours show a region of higher gas temperature at positions near the base of the traveling projectile. In Case 5, the total electrical energy consumed is 2.5 MJ. It is interesting to observe that, compared to the baseline (Case 1), where twice the electrical energy was expended, an increase of muzzle velocity of 6 m/s and a decrease of maximum pressure of nearly 30 MPa were achieved. This would indicate that reduction in electrical energy for equivalent performance is possible with appropriate positioning and timing of the plasma injections. The practical implication would be that the same performance could be realized with a smaller power supply. This is of interest since the size of the power supply is one of the limiting factors for fieldable weapon systems. Figure 9 shows the temperature contours for this case, and one can see that the temperature of the gas stream stays above 2,000 K at the projectile base for more than 4 ms. Case 6 (listed in Table 3) shows that an even higher performance increase can be obtained by changing the amount of electrical energy injected at a different injection position. In this case, the amount of electrical energy was increased along the barrel. Again, the maximum pressure decreased by approximately 30 MPa. In Figure 10, the temperature contours are plotted for this case, and the gas temperatures at the projectile base remain above 2,000 K until the projectile leaves the barrel. It is noted that barrel temperatures of this magnitude may have implications for erosion. In addition, it is assumed that the elastic strength profile of the gun tube can support the elevated pressures.

The results of the previous simulations imply that it is important to deposit the plasma energy as near as possible to the base of the projectile. This infers that the timing of the plasma pulse is critical. Only a finite time is available for an effective addition of electrical energy. Experimental time lags, including response time for a projectile position sensor and the response time of the pulse forming network (PFN), have to be considered. Too early injection of the plasma could have deleterious effects on the projectile and gun, and a late injection could result in a degraded performance. Figure 11 displays muzzle velocity vs. time curves for different single-injection positions (i.e., the electrical energy is injected at a single location). The maximum muzzle velocity is reached for each case when the plasma is injected as the base of the projectile just clears the injection port. As can be seen, the time window decreases with

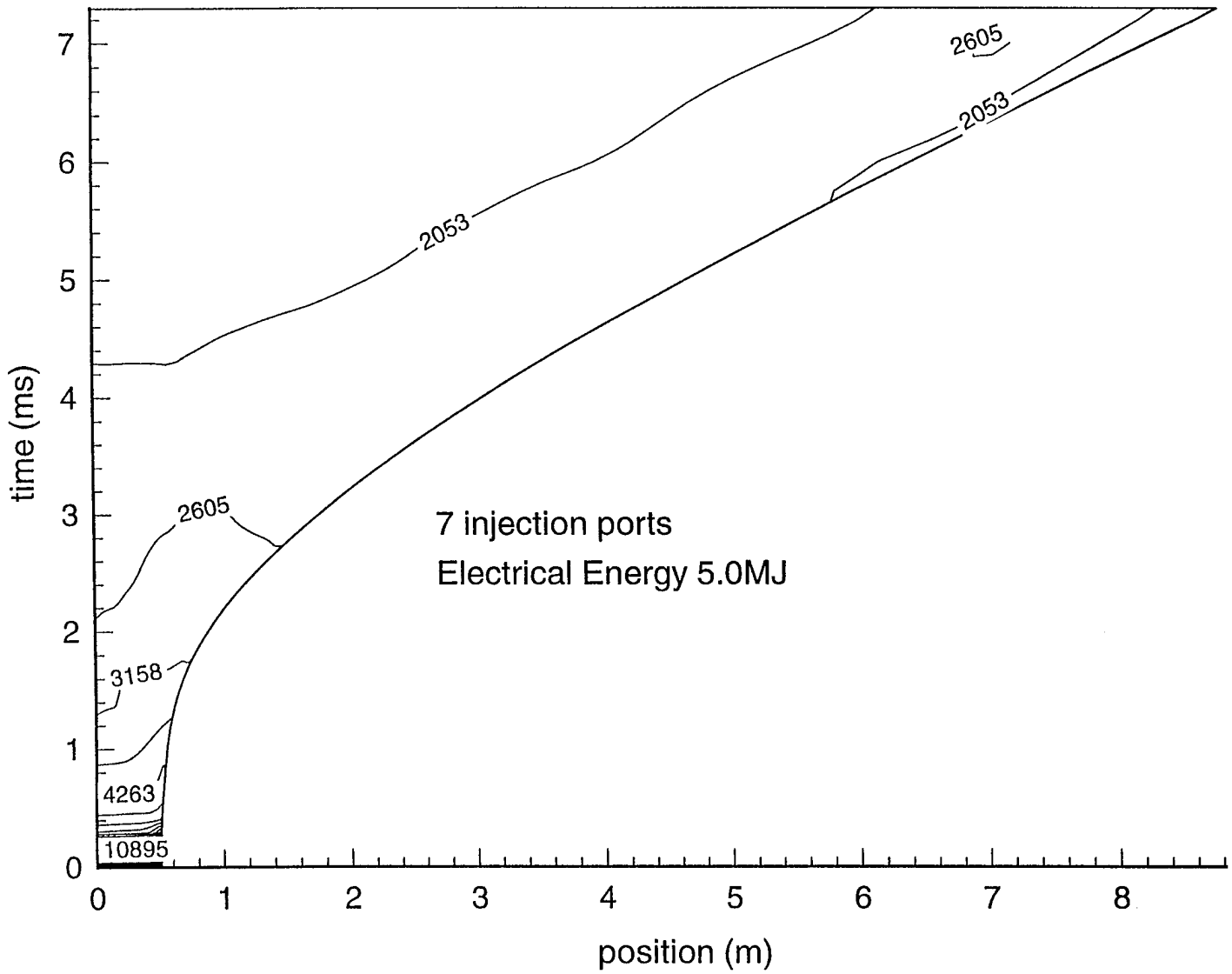

Figure 8. Temperature contours for seven injection ports; total electrical energy 5.0 MJ; case 4.

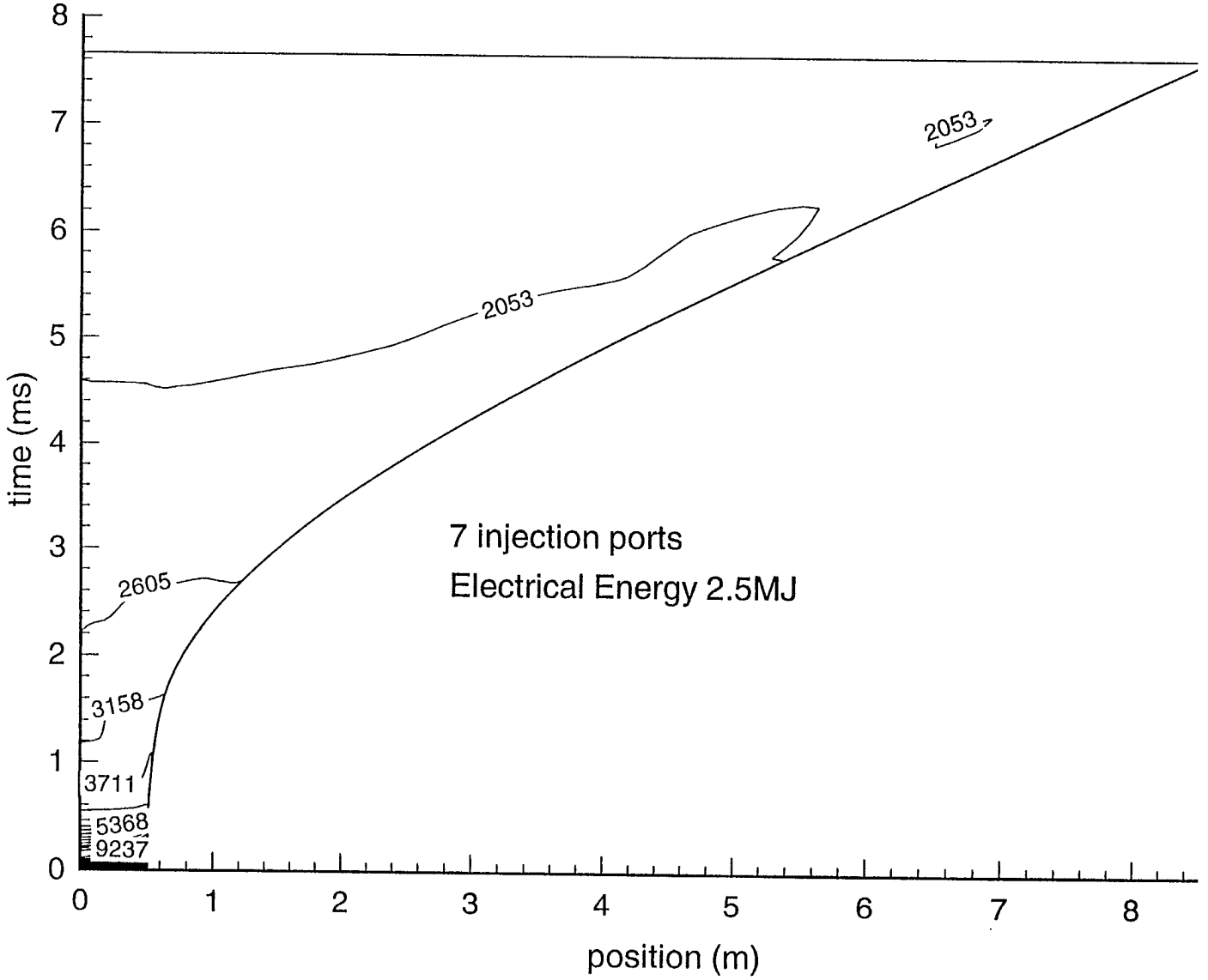

Figure 9. Temperature contours for seven injection ports; total electrical energy 2.5 MJ; case 5.

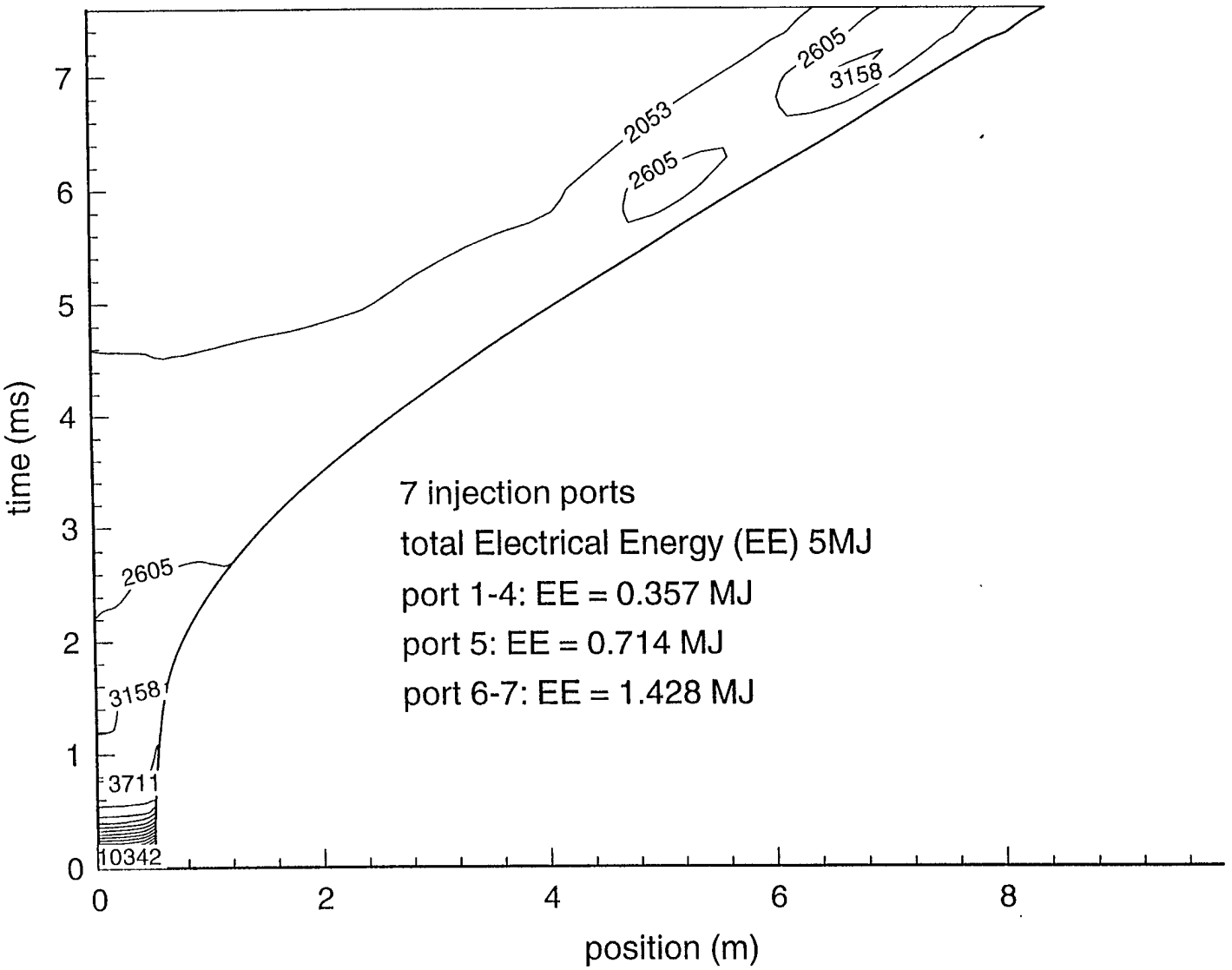

Figure 10. Temperature contours for seven injection ports; total electrical energy 5.0 MJ; case 6.

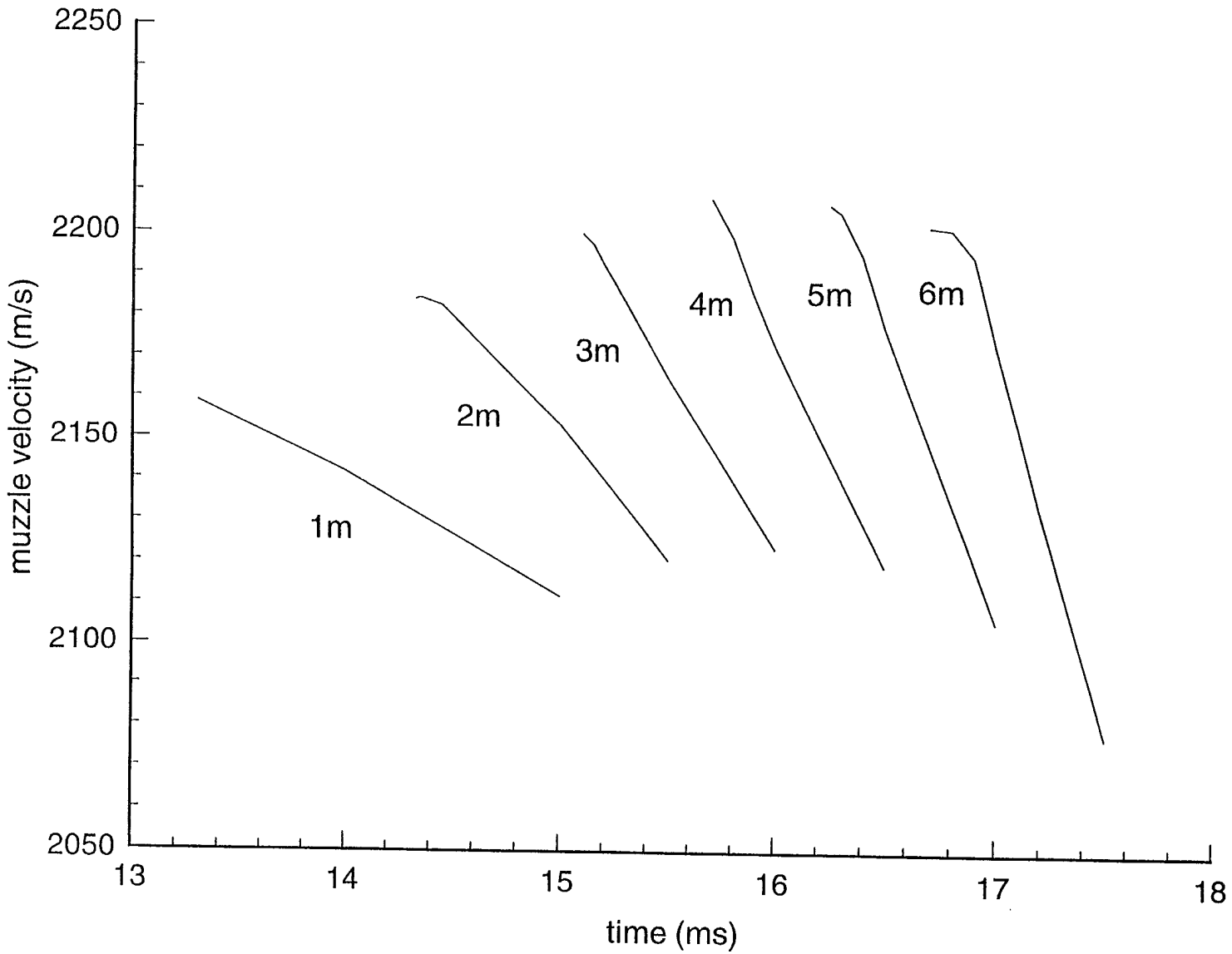

Figure 11. Injection windows.

increasing position of injection port since the projectile velocity increases with travel through the barrel. For example, the slope of the curve, and the subsequent sensitivity of muzzle velocity to time of plasma injection for the 6-m position is very steep. The muzzle velocity decreases from 2,202 to 2,078 m/s in a matter of 0.8 ms, which implies that a 0.8-ms delay in plasma injection would result in a 124-m/s muzzle velocity loss.

Plasma injection downbore can also result in high local temperatures and pressures, which have to be considered for experimental reasons. As already mentioned, high local gas temperatures in the gun barrel can have serious implications for gun erosion. Figure 12a shows the local gas temperature profiles for an injection position of 4 m. As one can see, the local temperature can reach in the order of 3,000 K. The predicted local pressure for the same injection location as seen in Figure 12b is approximately 250 MPa.

5. SPATIAL EFFECTS OF PLASMA

For the 2-D axisymetric simulation, the input data for the 105-mm baseline case were used to investigate spatial effects during the interior ballistic cycle. The solid propellant granules are loaded near the walls around a central ullage tube and uniformly distributed axially. In practice, the thin-walled central ullage tube serves to initially distribute plasma along the center line before the tube ruptures. In the simulation, this region is at ambient initially and, thus, the initial condition does not accurately reflect the experiment. However, the time of ullage tube rupture and the plasma conditions at this time are not well known. Thus, the model simplification appears to be a reasonable first approximation to the experiment.

Figures 13a–13h show the 2-D temperature profiles for various time steps. The y-axis depicts the radial position, and the x-axis the axial position (center line). The temperature is plotted in a logarithmic dimensionless scale, normalized with the plasma temperature (15,000 K) in order to provide better display of the results. The plasma is injected from the breech end into a ullage tube. The propellant is loaded around the ullage tube, and the initial pressure ratio between the region external to the ullage tube and the ullage tube is assumed to be 0.1. At time zero, the plasma injection begins from the breech. The plasma expands rapidly, radially, cooling and creating a region of turbulence at the breech end, as can be seen on the temperature contours a–c. The hot gas impacts the projectile base, where it stagnates and is reflected. A hotter region associated with the plasma can be observed for the first few time frames (Figure 13a–13c) at the projectile end. During approximately the first 2 ms, the plasma energy input is

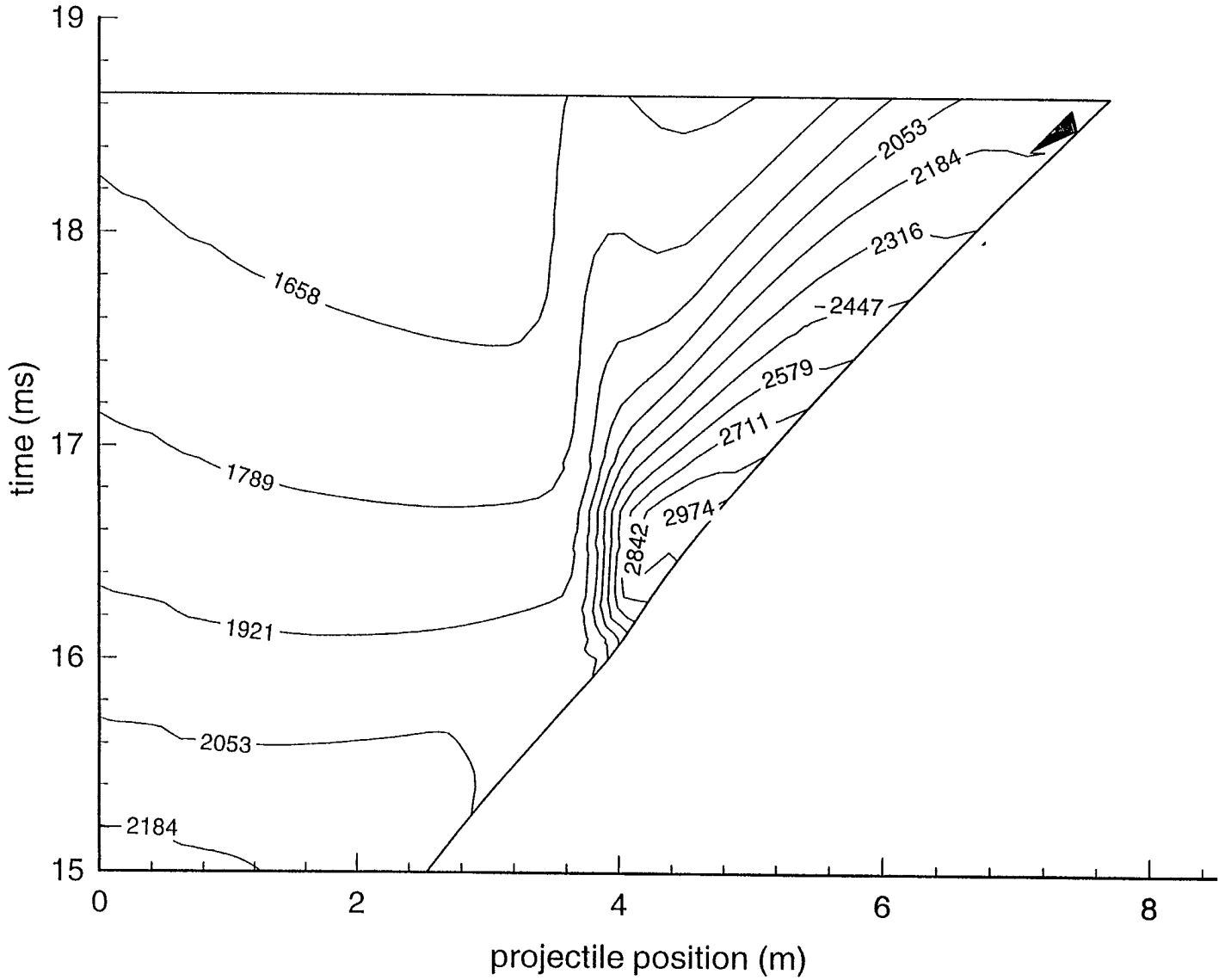

Figure 12a. Temperature contours for injection position 4 m.

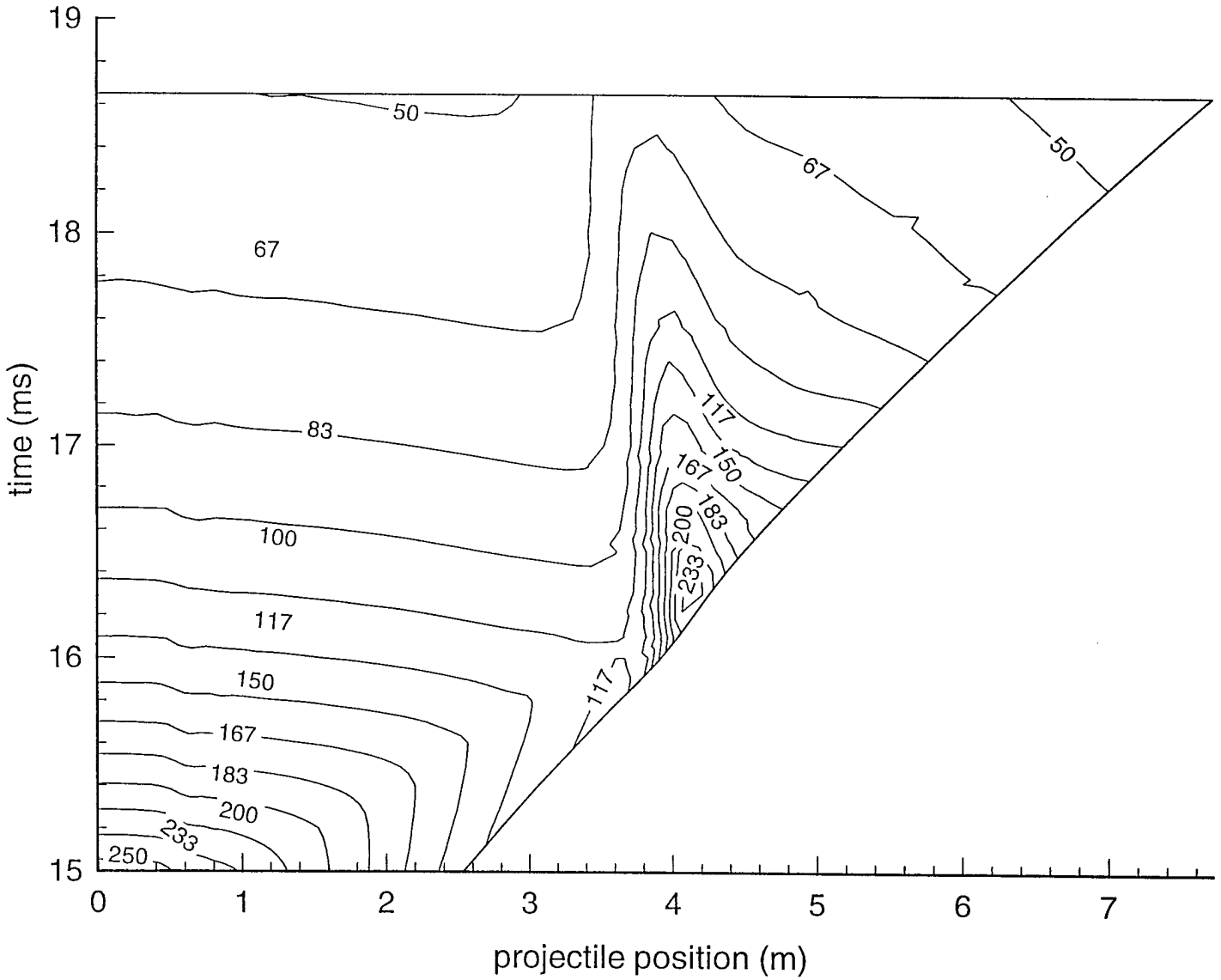

Figure 12b. Pressure contours for injection position 4 m.

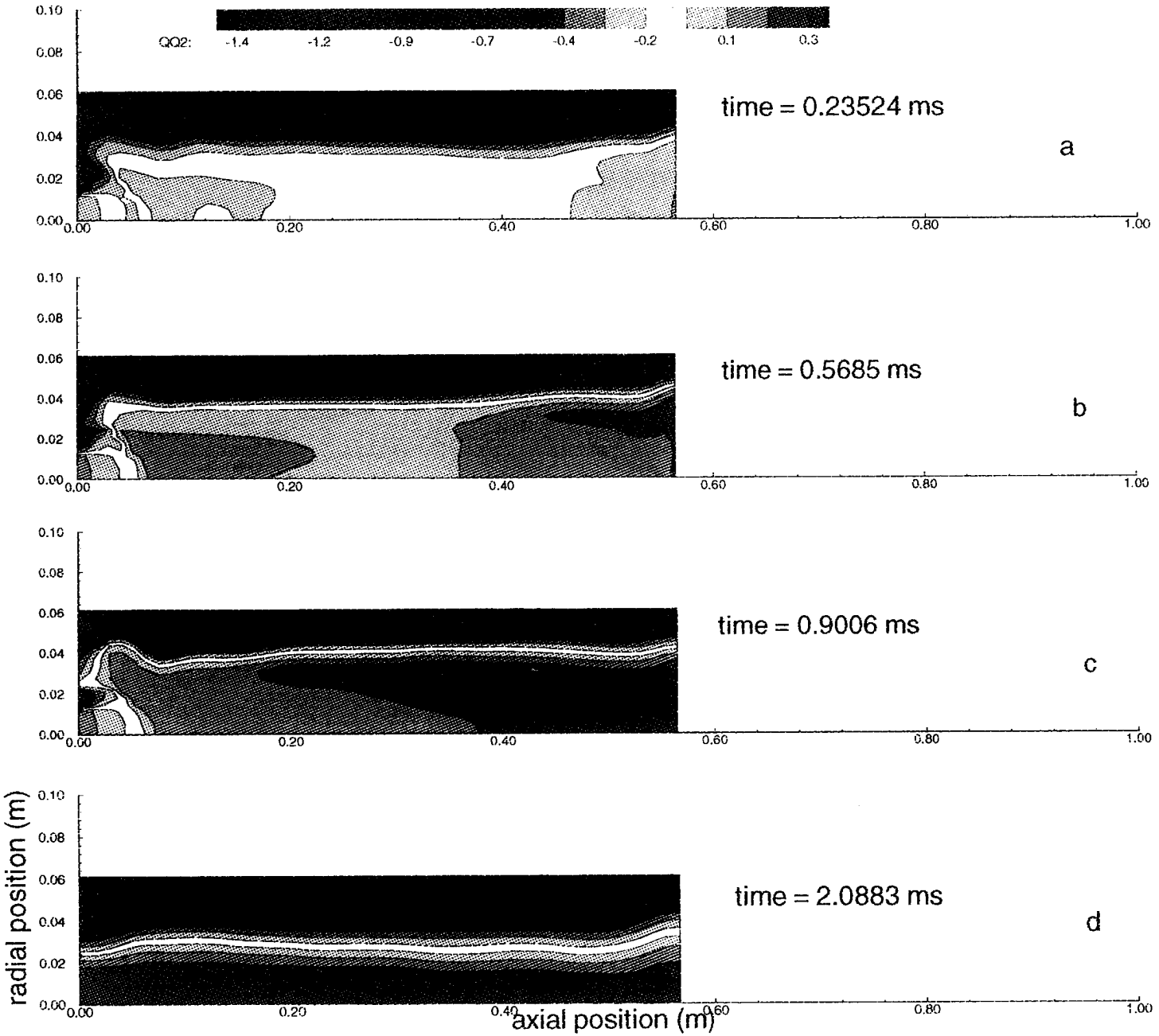

Figure 13. Nondimensional logarithmic temperature contours; CRAFT model predictions.

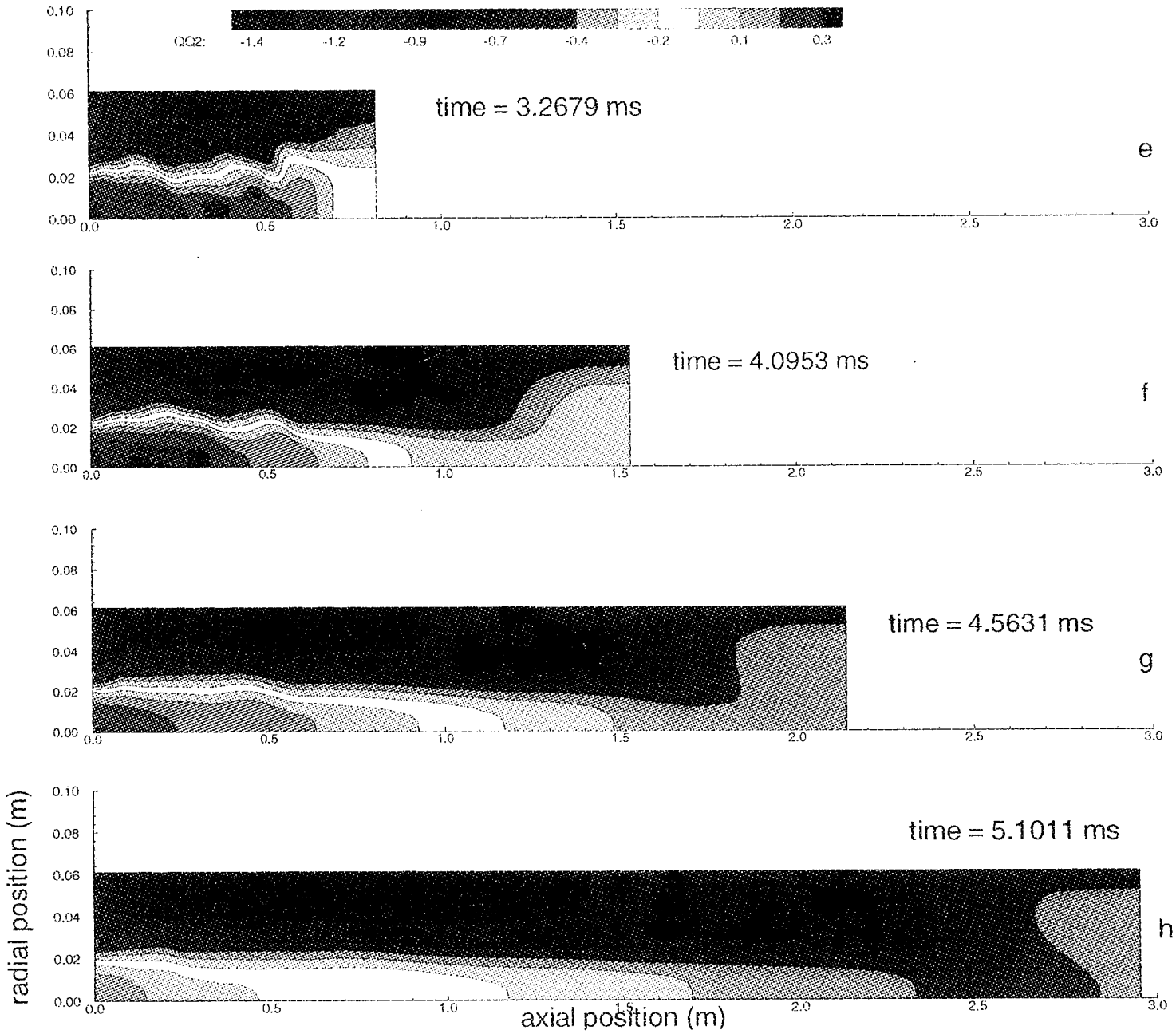

Figure 13. Nondimensional logarithmic temperature contours; CRAFT model predictions (cont.).

low, based on experimental data, and the plasma is used primarily as an ignition stimulus. In the later stages of plasma injection (>2 ms), a higher current input results in an increase of electrical energy, so an augmentation of the chemical energy with electrical energy takes place. From approximately 2 ms onward (Figure 13d), a hot plasma core can be noticed surrounded by the much cooler propellant bed. The temperature profile indicated that heat transfer and ignition of the propellant bed has also occurred, and a strong radial temperature gradient is indicated. The original projectile position is 0.57 m, and at 3.268 ms (Figure 13a), the projectile has been engraved and has started to move. The plasma is reflected from the projectile base, and a wavy structure near the breech can be seen in the temperature profiles. The wave form can be observed till approximately 5.1 ms. The structure is thought to be due to a combination of a rarefaction wave and vigorous plasma injection. As can be concluded from Figures 13e–13h, the plasma needs a finite time to propagate through the gas and combustion products. At the later stages of the interior ballistic cycle (4.5 and 5.1 ms), the plasma-heated combustion products no longer reach the projectile base. This confirms the predictions of the 1-D model.

A strong temperature gradient in radial direction for all time steps can also be observed. The figures suggest that the plasma products do not reach the chamber walls and have only a local influence. This has some advantage, since the temperature at the chamber walls is not high enough to cause serious erosion of the gun tube. However, the cool regions at the chamber walls suggest lower local burning rates, and this is confirmed by the next figures. Figures 14a and 14b depict the grain positions and nondimensionalized particle diameters which are tracked through the Lagrangian formulation through the entire interior ballistic cycle. The nondimensional grain diameters are the equivalent of unburned fractions of the propellant grains. Two different time steps have been plotted. In Figure 14a (3.268 ms), the projectile has started to move and the propellant bed is fluidized. A strong radial gradient in unburned propellant fraction can be observed, where the larger particle diameters are at the wall which is outside the influence region of the plasma. The wavy structure at the breech seen in the temperature profile (Figure 13e) is repeated in the particle profile. A cool wall temperature region at the wall between approximately 0.2- and 0.6-m axial position results in a region of low burning rate, as can be seen in the large number of unburned or only slightly burnt particles in that region. In Figure 14b this trend is continued; again a local region of particles with lower fractions of burnt propellant can be observed at the wall. This would suggest that the interior ballistic process in that region is not very efficient, and changes in plasma injection should be made to increase performance. By injecting the plasma not only in an axial but in a radial direction, the low temperature zones could possibly be avoided.

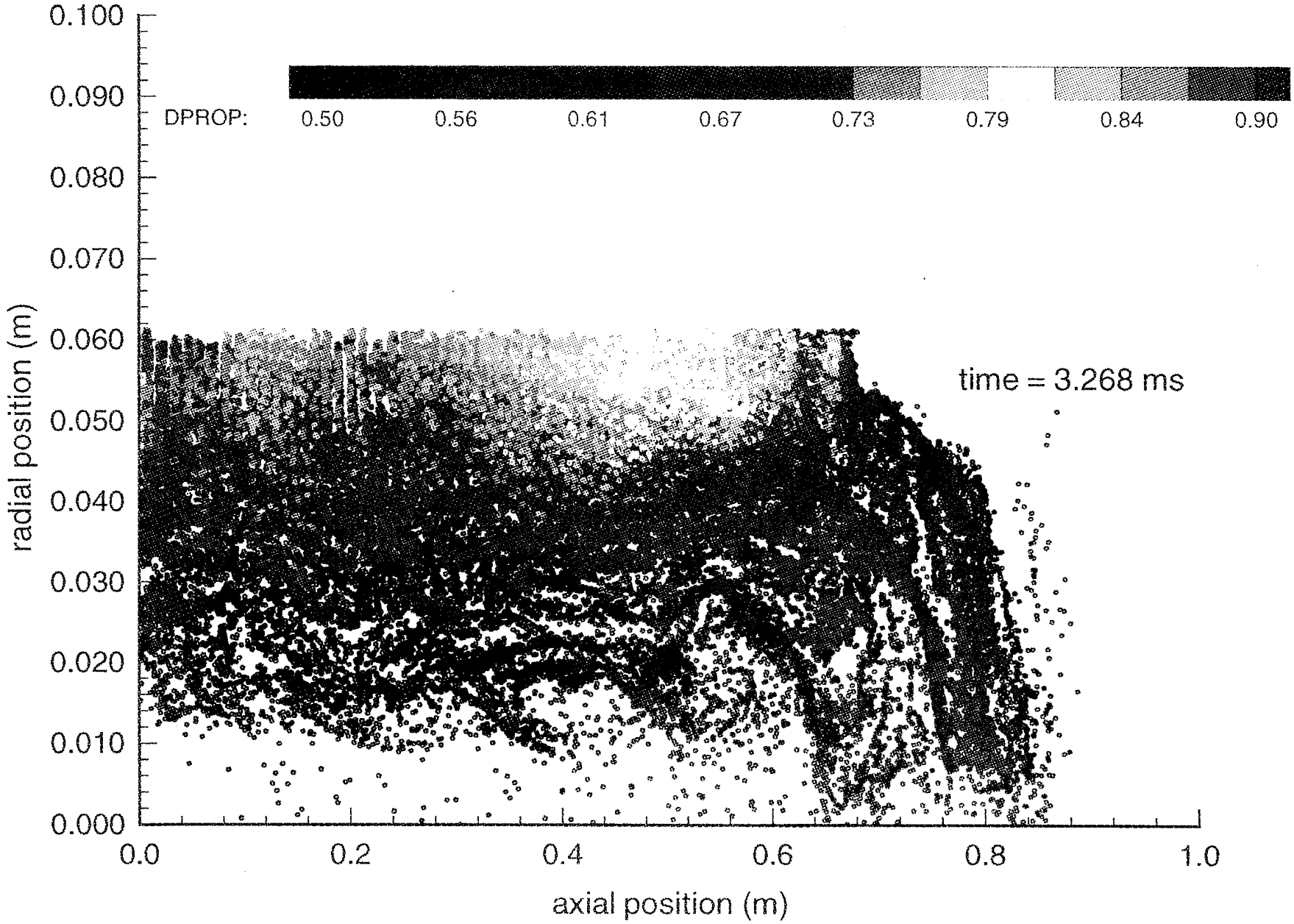

Figure 14a. Particle positions and diameters at time = 3.268 ms; CRAFT model predictions.

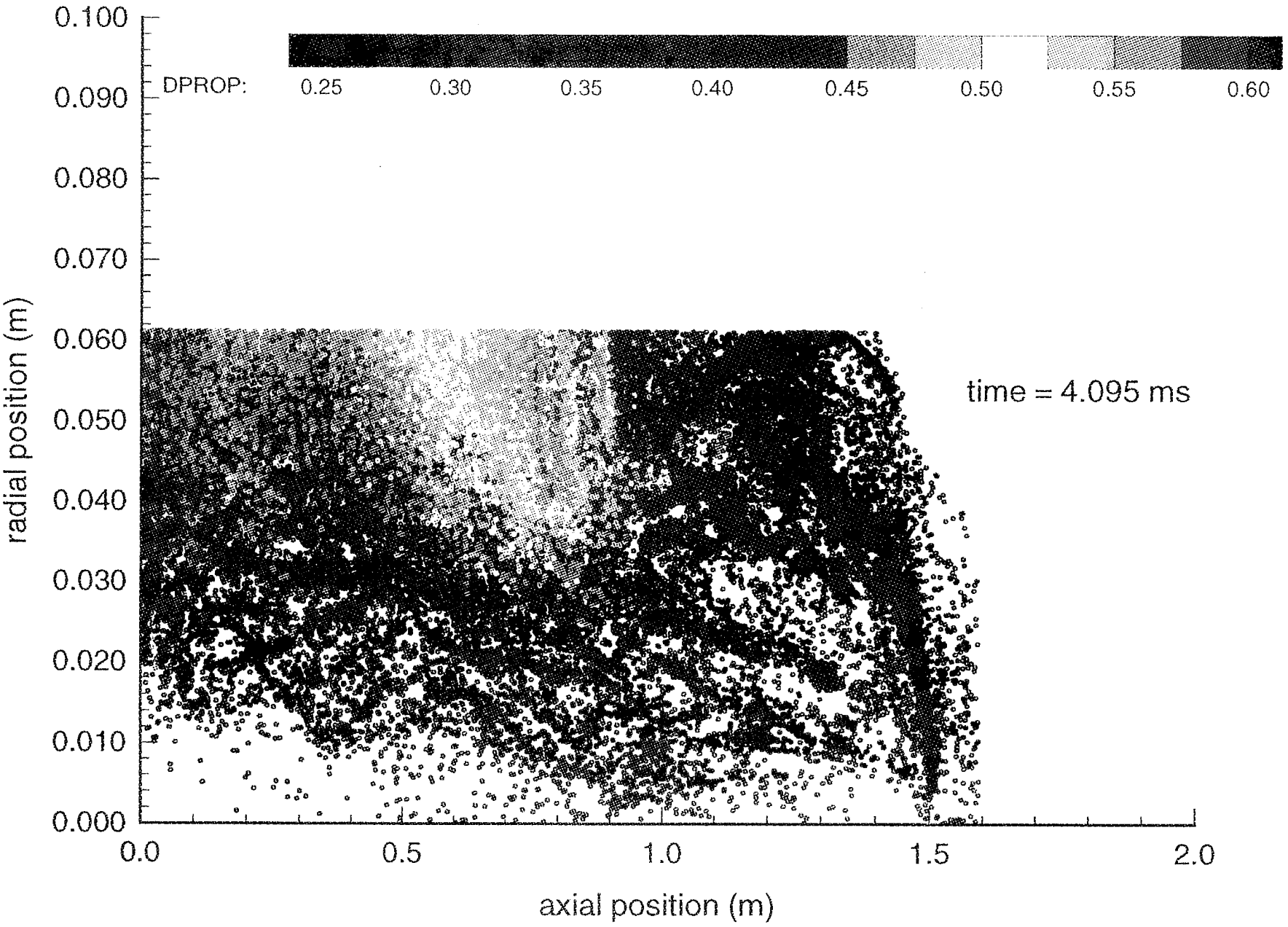

Figure 14b. Particle positions and diameters at time = 4.095 ms; CRAFT model predictions.

Figure 15 shows a comparison of the pressure-time curve of CRAFT model predictions and experimental data. A reasonable agreement can be observed. The initial pressure rise between model predictions and experimental data is nearly identical. The width of the curve is smaller for the CRAFT predictions. During approximately 3–5 ms, plasma injection is strong in the experiment. In addition, precise constituents of the plasma are not known as well as particulars such as ullage tube dimensions. It is known, however, that the numerical results are sensitive to the plasma properties. Thus, improvement in the plasma submodule is expected to be needed to accurately describe the experiment.

6. CONCLUSIONS

The investigation is based on an experimental ETC gun firing and extended to considered a number of plasma injection related parameters. The comparisons of experimental data with model predictions are in good agreement.

The 1-D parametric study revealed that there is a cutoff point in the interior ballistic cycle of high-velocity projectiles where additional electrical energy input does not result in a projectile velocity increase when the plasma is introduced at the breech of the gun. In order for the plasma-heated combustion gases to reach the base of the traveling projectile and result in an increase of projectile kinetic energy, the duration of the plasma injection, the amount of electrical energy, as well as the region and timing of the injection are important.

Simulations with the 2-D CRAFT code show that strong spatial effects can be observed in the temperature and the diameter profiles. The simulations suggest that the breech-injected plasma has only local influence and propellant regions of less efficient burning are created. Changes in the plasma injection, which allow axial and radial penetration of the plasma jet into the propellant bed, is expected to eliminate local regions of poorly burnt propellant.

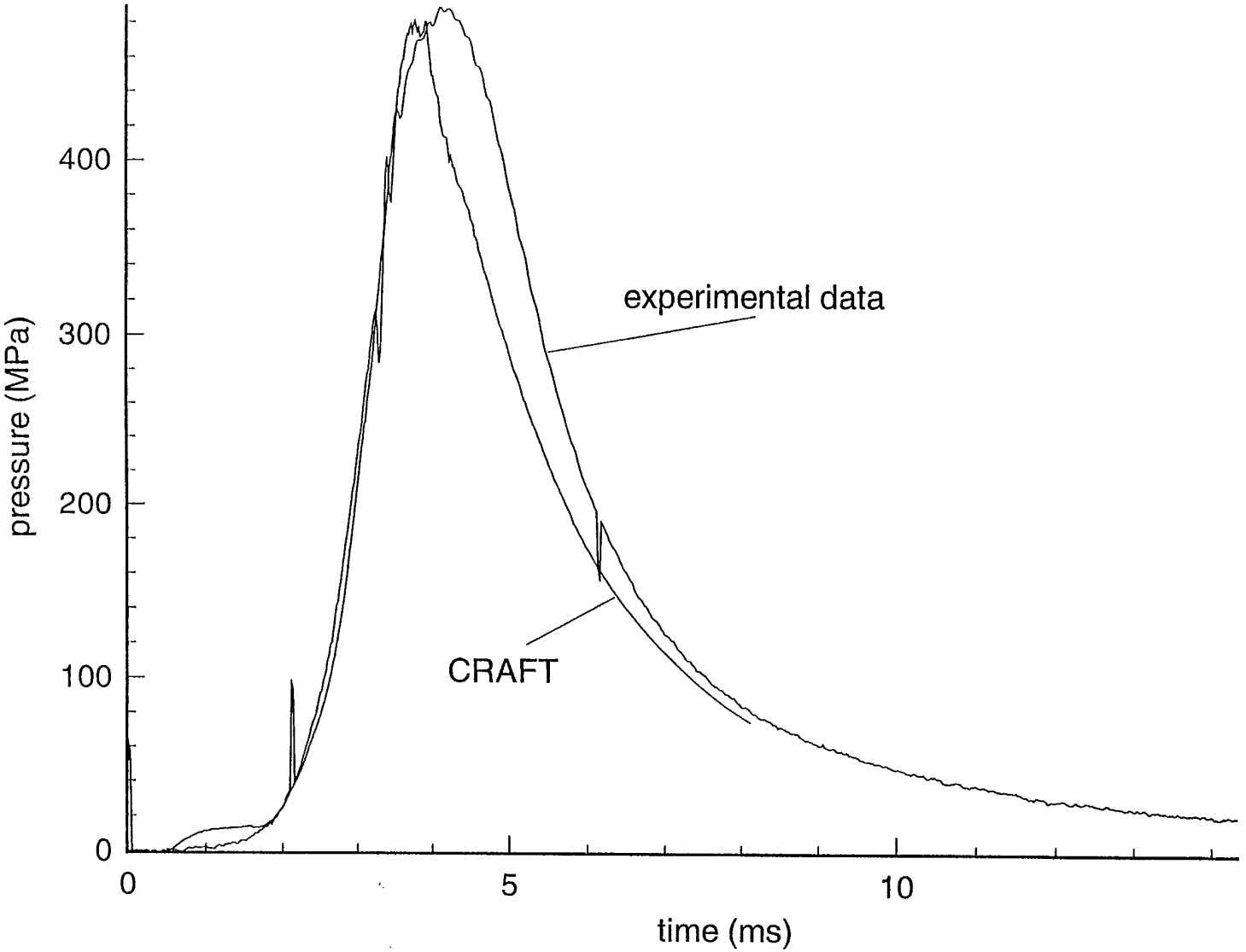

Figure 15. Comparison of experimental data and CRAFT model predictions.

7. REFERENCES

Edwards, C. M., M. A. Bourham, and G. Gilligan. "Experimental Studies of the Plasma Propellant Interface for Electrothermal-Chemical Launchers." Seventh Electromagnetic Launch Symposium, in IEE Transactions on Magnetics, vol. 31, No. 1, pp. 404–409, January 1995.

Ernhart, J. N., N. Winsor, and G. P. Wren. "Electrothermal-Chemical (ETC) Extensions to IBHVG2 With a New User's Tutorial." ARL-TR-348, U.S. Army Research Laboratory, Aberdeen Proving Ground, MD, January 1994.

Glick, R. L. "Temperature Sensitivity of Solid Propellant Burning Rate." AIAA Journal, vol. 5, pp. 586–587, 1967.

Gough, P. S. "Interior Ballistics of Guns." Progress in Astronautics and Aeronautics, vol. 66, pp. 176–196. Edited by H. Krier and M. Summerfield. New York: AIAA, 1979.

Gough, P. S. "XNOVA–An Express Version of the NOVA Code." PGS-TR-83-5, Naval Ordnance Station, Indian Head, MD, 1983.

Hosangadi, A., N. Sinha, and S. M. Dash. "Multi-dimensional Simulation of ETC Gun Flowfields." SAIC/FW TR-121, Science Applications International Corporation, Ft. Washington, PA, February 1994.

Juhasz, A. A., J. O. Doali, and R. E. Bowman. "Wide Temperature Range Burning Rate Studies of M30A1 Propellant." 18th JANNAF Combustion Meeting, in CPIA Publication 347, vol. 2, pp. 13–23, October 1981.

Kaplan, Z., D. Melnik, M. Sudai, D. Plotnik, G. Applebaum, D. Kimhe, R. Alimi, L. Perlmutter, A. Juhasz, P. Tran, and J. Brown. "A Field Study of Hypervelocity Solid Propellant Electrothermal 105-mm Launcher." IEEE Transactions on Magnets, vol. 31, pp. 425–430, January 1995.

Powell, J. D., and A. E. Zielinski. "Theory and Experiment for an Ablating Capillary Discharge and Applications to Electrothermal-Chemical Guns." BRL-TR-3355, U.S. Army Ballistic Research Laboratory, Aberdeen Proving Ground, MD, July 1992.

White, K. J., W. F. Oberle, A. A. Juhasz, I. C. Stobie, K. Nekula, G. I. Katulka, and S. Driesen. "Electrothermal-Chemical Propulsion With High Loading Density Charges." U.S. Army Research Laboratory, Aberdeen Proving Ground, MD, ARL-TR-845, August 1995.

Wren, G. P., W. F. Oberle, K. N. Winsor, A. Hosangadi. "Spatial Effects of an Electrically Generated Plasma on the Interior Ballistics of Electrothermal-Chemical (ETC) Guns." IEE Transactions on Magnetics, vol. 31, no. 1, pp. 457–462, January 1995.

INTENTIONALLY LEFT BLANK.

APPENDIX:

INPUT INFORMATION FOR CODES

INTENTIONALLY LEFT BLANK.

```
$COMM
        105mm SOREQ contract - Shot16 from Eglin AFB firings
        D2 channel Projectile, Mass=3.862 kg, Power based on experiment
        EGLIN M30, HEX 19 perf propellant, FROM RADFORD, 6.3kg
        No Chambrage, Smooth bore gun
        Use with IB504 program, Metric input, Metric Output
$INFO
        POPT=1,1,1,0,0
        RUN='Shot 16 (105 mm) - IBHVG2.ETC'
        GRAD=1
$GUN
        NAME='105MM GUN'
        CHAM=.006704 GRVE=0.105 LAND=0.105  $SMOOTH BORE
        TRAV=9.158  TWST=99
$PRIM
        NAME='DUMMY'  CHWT=.001573966
        GAMA=1.267  FORC=918827.1 COV=.001106  TEMP=2449
$PROP
        NAME='EGLIN M30' CHWT=6.3  GRAN='19HX'
        LEN=.01283 DIAM=.0101854  PD=.0005334  WI=.001274
        WM=.001273 WO=.001211 RHO=1672.8
        GAMA=1.2530  FORC=1077600 COV=.000968  TEMP=3025.
        NTBL=-4
        PR4L=30.,60.58,151.45,654.34
        CF4L=0.000119,.00276069,.00511511,.00411458
        EX4L=1.67,.7843,.6100,.6649
        EROS=.000
$PROJ
        NAME='105MM SLUG' PRWT=3.862
$RESI
        NPTS=4  AIR=1
        TRAV=0., .04, .05, 9.16
        PRES=10.,10., .0, .0
$HEAT
        TSHL=0.0001143   CSHL=460.316  RSHL=7861.09
        TWAL=293         H0=11.348     HL=1
$ETC
        NPWR=12
        TPWR=0.0,0.596E-3,1.0460E-3,1.472E-3,1.736E-3,2.154E-3,
             2.470E-3,3.028E-3,3.462E-3,3.654E-3,4.33E-3,5.33E-3
        PWR=0.E6,86.632E6,88.824E6 ,27.68E6,152.986E6,192.241E6,
            433.348E6,517.039E6,755.755E6,746.788E6,286.094E6,0.0
$END
```

```
Shot 16 (105mm) - XKTC.ETC
TTFFTFT0000000010400000000000001
   50 1000    010000    0   0  0.0001
10.0       360.55    0.0001     2.0       0.05      0.01      0.0001     0.0001
    5    0    0    4    0    0    1    4    0    0    0    2
    0
550.       14.7      28.896    1.4
550.0
EGLIN M30              0.0       20.0      13.889    .060434
   15    0.401     0.021   0.50512      19.       0.      0       0.     0
78740.     1.0       0.
   4350.  1.8380e-6   1.67      8786.39  0.002192    0.7843  21965.97  0.009672
    0.610  94904.     0.00592    0.6649     0.0      550.    0.019996  0.0001
   0.6
17099464.6  23.34     1.2530    26.79
   0.00      2.56      3.937      2.524     15.748   2.393      22.440   2.0669
  360.55    2.0669
 22.441      2900.     25.196      2900.     25.59     0.        360.55       0.
1.4          14.7      550.0     28.896
7.77        0.0228    .7
 22.441      8.514     18.18     0.000
 3.937       15.748
    1    1    0    0
    0   12
13046002.7  0.011      0.40      1.4       10.0
0.0         22.441     0.0
0.0         0.0        0.0       0.0       0.0       0.0       0.0
0.596      0.019722  0.019722    0.0       0.0       0.0       0.0
1.046      0.047208  0.047208    0.0       0.0       0.0       0.0
1.472      0.077307  0.077307    0.0       0.0       0.0       0.0
1.736      0.101655  0.101655    0.0       0.0       0.0       0.0
2.154      0.154064  0.154064    0.0       0.0       0.0       0.0
2.470      0.226011  0.226011    0.0       0.0       0.0       0.0
3.028      0.402775  0.402775    0.0       0.0       0.0       0.0
3.462      0.577870  0.577870    0.0       0.0       0.0       0.0
3.654      0.670950  0.670950    0.0       0.0       0.0       0.0
4.33       0.909837  0.909837    0.0       0.0       0.0       0.0
5.33       1.000000  1.000000    0.0       0.0       0.0       0.0
```

```
&INPUT
 NITER=0250, IDIMEN=2, IAXISY=1, NEIG=1, IPLOT=1,
 IREADG=1, IREADQ=0, IOUT=0250,
 ITMAX=1, TVD=2.0, EPU=1.0, EPC=0.1, PHIOSH=0.33333333,
 RINFD=3.0, QINFD=1.0, TINFD=15000.0,
 CFL=0.5, PITCH=0.0, YAW=0.0
 IMODEL=3, IVISC=0, ITURB=0, IKEW=0,
 PHGINF=0.99999,
 PRSINF=1.E+06, PINRAT=1.00,
 ACCEL=0.0, AMASS=3.862, UWALL=0.0, XWALL=0.0,
 IHIS=0, ISAV=25, CINFL=0.8, 0.2,
 JDIAPH=09, IDIAPH=50,
 PRAT=0.1, TRAT=0.033333, ITACC=1,
 PHGCHM= 0.99999, 0.99999, 0.99999,
 PBACK=1.E+06,
 DELXMX=0.012, ITHERMP=1, YPLASM=7.5E-03,
 &END
&BCS
 IBCL=2, IBCU=2, JBCL=2, JBCU=2, KBCL=1, KBCU=1,
 ILSYM=0,IUSYM=0,JLSYM=1,JUSYM=0,KLSYM=0,KUSYM=0,
 ILGOS=0, IUGOS=0, JLGOS=0, JUGOS=0, KLGOS=0, KUGOS=0,
 INPLAS=1,
&END
&PART
 ROPROP=1672.6966, CSPROD=0.0,1.0,0.0
 GL=0.01283, PD=0.0005334, WI=0.001253066, WO=0.001253066,
 CPPINF=1684.5, TIGN=350.0, GEPSINF=1.0,
  ENPROP=4259.288538E+03, 4259.288538E+03, 4259.288538E+03,
  4259.288538E+03, 4259.288538E+03, 4259.288538E+03, 4259.288538E+03,
  FRLAY=1.0, 0.9503, 0.9006, 0.8510, 0.8013, 0.7516, 0.7218,
  NLAY=7, TPINF=293.0, IDIAM=1, CFLP=0.1,
  ILAW=0, IPROP=50, JPROP=10,
  PMASS1=5.915, PMASS2=0.265, PMASS3=0.120,
&END
```

```
C*********************************************************************C
      BLOCK DATA
      INCLUDE 'CRAFT.CMN'
      COMMON/A01/  X(LI,LJ,LK),Y(LI,LJ,LK),Z(LI,LJ,LK),VOL(LI,LJ,LK)
      COMMON/A02/  XI(LI,LJ,LK,3),YI(LI,LJ,LK,3),ZI(LI,LJ,LK,3),
     >VOLNW(LI,LJ,LK),XNW(LI,LJ,LK),YNW(LI,LJ,LK),ZNW(LI,LJ,LK),
     > VOLOL(LI,LJ,LK),VXFAC(LI,LJ,LK),VYFAC(LI,LJ,LK),VZFAC(LI,LJ,LK)
     >          ,GEPS(LI,LJ,LK),GEPSO(LI,LJ,LK),GEPSINF
      COMMON/A03/  IDIMEN,IMAX,IMAX1,IMAX2,JMAX,JMAX1,JMAX2,
     >             KMAX,KMAX1,KMAX2
      COMMON/A04/  Q(LI,LJ,LK,LN),QO(LI,LJ,LK,LM),S(LI,LJ,LK,LM),
     >             QOL(LI,LJ,LK,LN),PTGZ(LI,LJ,LK,4),ZD(LI,LJ,LK,LS),
     >          PHBC(LI,LJ,LK,3),CTSPD(LI,LJ,LK,LS),CTCON(LI,LJ,LK,2)
      COMMON/A05/IREADQ,IREADG,IOUT,NEIG,ITMAX,NITER,ITER,IVISC,ITACC,
     >      IAXISY,ITURB,ICATL,ITEMP,UINFL(LJ),TINFL,PINFL,CINFL(LS),
     > IKEW,IPLOT,XWALL,ACCEL,UWALL,AMASS,PBACK,LJET,MJET,PRAT,TRAT
      COMMON/A06/  TAU,DTAU,CFL,TVD,EPU,EPC,PHIOSH
      COMMON/A07/  NEQ,NS,NSP4,NSP5,NSM,NBLK,NCTB,IELEC,IMODEL
      COMMON/A08/ZMW(LS),DMW(LS),TBE(LT,LS),ZMU(LS,3),RRF(LE,3),RRV(3),
     >      ZKSP(LS),RRB(LE,3),HOF(LS),NUR(LE,LR),NUP(LE,LR),IONS(LS)
      COMMON/A09/  TTB(100),CPTB(100,LS),CPFTB(100,LS),NTABLE
     >   ,TTV(100),BVTB(100,LS),CVTB(100,LS),NVTBLE,ITHERMP
      COMMON/A10/  RINFD,TINFD,CSINF(LS),UINF,VINF,WINF,QINFD,ZMWIFD,
     > RGASD,BETA1,BETA2,BETA3,RE,HINF,GAMINF,DSINF(LS),PHGINF,PRSINF,
     > RINF,TINF,BMXINF,CMXINF,ZMXINF,CTSINF(LS),
     > ZMUIFD,ZKINFD,ZDINFD,TWALLD,EMSVTY,XKINF,XEINF
      COMMON/A11/  PITCH,YAW
      COMMON/A12/  CP(LS),CPF(LS)
      COMMON/A13/  SFCP(100,LS),SFCPF(100,LS),SFBV(100,LS),SFCV(100,LS)
      COMMON/A26/  QGOS(LL,LL,LN,LB),QOGOS(LL,LL,LM,LB),
     >   PTGOS(LL,LL,4,LB),ZDGOS(LL,LL,LS,LB),PHGOS(LL,LL,LS,LB),
     >  CTSGOS(LL,LL,LS,LB),CTNGOS(LL,LL,2,LB),ALPGOS(LL,LL,LB),
     >  QG0(7),QG1(7),QGS0(LS,2),QGS1(LS,2),ISONIC
      COMMON/A27/STAGP,STAGH,ILGOS,IUGOS,JLGOS,JUGOS,KLGOS,KUGOS,INPLAS
      COMMON/A28/ IMAXIN,DELXMX,
     > INCRM
C*
      COMMON/ACURR/NCURR,CURR(200),CTIM(200)
C*
C* UNIVERSAL GAS CONSTANT
      DATA RGASD /8314.34/
C* SPECIES MOLECULAR MASS (KG/KMOL)
      DATA (DMW(N),N=1, 3)
     #/ 4.675, 23.34, 23.34  /
C* ION FLAGS (0 - NEUTRAL, 1,2,3,... -VE CHARGE )
      DATA (IONS(N),N=1, 3)
     #/ 0,0,0  /
C* HEAT OF FORMATION
      DATA (HOF(N),N=1, 3)
     #/ 0.0, 0.0, 0.0 /
C* REACTANT AND PRODUCT STOICHIOMETRIC COEFICIENTS
C      DATA ((NUR(N,L),L=1,5),(NUP(N,L),L=1,5),N=1,1)
C*   30 PROP = 10CO2 + 14 N2 + 51 H2O
C     1/ 0,   0,   0,   0, 30,
C     1  0,  10,  14,  51,  0 /
C       C    C    N    H  P
C            O    2    2  R
C            2         O  O
C                      P
C* THIRD BODY EFFICIENCIES
C      DATA ((TBE(M,N),N=1,5),M=1,1)
C     1/0., 0., 0., 0., 0. /
C* VISCOSITY CURVE FIT COEFFICIENTS  (SUTHERLAND'S LAW)
      DATA ((ZMU(M,N),N=1,3),M=1,3)
     1 / 0.0268142,  0.3177838, -11.3155513,
     2   0.0268142,  0.3177838, -11.3155513,
```

```
     3   0.0268142,   0.3177838, -11.3155513 /
C*
C        DATA ZKSP(6) /0.6571112/
C* FORWARD REACTION RATES
       DATA ((RRF(M,N),N=1,3),M=1,1)
     1/6.25E+05, -4000.0, 0.0 /
C    1/7.5E+05, -4000.0, 0.0 /
C    1/5.0E+05, -4000.0, 0.0 /
C     1/ 1.0,    -10000000.0, 0.0 /
       DATA (RRV(N),N=1,3)
     1/1.25E+06, -4000.0, 0.0 /
C    1/1.5E+06, -4000.0, 0.0 /
C    1/1.0E+06, -4000.0, 0.0 /
C* BACKWARD REACTION RATES
       DATA ((RRB(M,N),N=1,3),M=1,1)
     1/ 1.0,    -10000000.0, 0.0 /
C
C* TEMPERATURE TABLE
C
       DATA (TTB(N),N=1,50)
     >/    0.0,   400.0,   800.0,  1200.0,  1600.0,
     >  2000.0,  2400.0,  2800.0,  3200.0,  3600.0,
     >  4000.0,  4400.0,  4800.0,  5200.0,  5600.0,
     >  6000.0,  6400.0,  6800.0,  7200.0,  7600.0,
     >  8000.0,  8400.0,  8800.0,  9200.0,  9600.0,
     > 10000.0, 10400.0, 10800.0, 11200.0, 11600.0,
     > 12000.0, 12400.0, 12800.0, 13200.0, 13600.0,
     > 14000.0, 14400.0, 14800.0, 15200.0, 15600.0,
     > 16000.0, 16500.0, 17500.0, 18500.0, 20000.0,
     > 30000.0, 50000.0, 70000.0, 90000.0,110000.0 /
C
C* SPECIES ENTHALPY TABLES (CALORICALLY IMPERFECT)
C*
C
       DATA (CPTB(N, 1),N=1,50)
     #/ 9235.36,  9235.36,  9235.36,  9235.36, 9235.36,
     #  9235.36,  9235.36,  9235.36,  9235.36, 9235.36,
     #  9235.36,  9235.36,  9235.36,  9235.36, 9235.36,
     #  9235.36,  9235.36,  9235.36,  9235.36, 9235.36,
     #  9235.36,  9235.36,  9235.36,  9235.36, 9235.36,
     #  9235.36,  9235.36,  9235.36,  9235.36, 9235.36,
     #  9235.36,  9235.36,  9235.36,  9235.36, 9235.36,
     #  9235.36,  9235.36,  9235.36,  9235.36, 9235.36,
     #  9235.36,  9235.36,  9235.36,  9235.36, 9235.36,
     #  9235.36,  9235.36,  9235.36,  9235.36, 9235.36 /
C
       DATA (CPTB(N, 2),N=1,50)
     #/ 1764.239244, 1764.239244, 1764.239244, 1764.239244, 1764.239244,
     #  1764.239244, 1764.239244, 1764.239244, 1764.239244, 1764.239244,
     #  1764.239244, 1764.239244, 1764.239244, 1764.239244, 1764.239244,
     #  1764.239244, 1764.239244, 1764.239244, 1764.239244, 1764.239244,
     #  1764.239244, 1764.239244, 1764.239244, 1764.239244, 1764.239244,
     #  1764.239244, 1764.239244, 1764.239244, 1764.239244, 1764.239244,
     #  1764.239244, 1764.239244, 1764.239244, 1764.239244, 1764.239244,
     #  1764.239244, 1764.239244, 1764.239244, 1764.239244, 1764.239244,
     #  1764.239244, 1764.239244, 1764.239244, 1764.239244, 1764.239244,
     #  1764.239244, 1764.239244, 1764.239244, 1764.239244, 1764.239244/
C
       DATA (CPTB(N, 3),N=1,50)
     #/ 1764.239244, 1764.239244, 1764.239244, 1764.239244, 1764.239244,
     #  1764.239244, 1764.239244, 1764.239244, 1764.239244, 1764.239244,
     #  1764.239244, 1764.239244, 1764.239244, 1764.239244, 1764.239244,
     #  1764.239244, 1764.239244, 1764.239244, 1764.239244, 1764.239244,
     #  1764.239244, 1764.239244, 1764.239244, 1764.239244, 1764.239244,
     #  1764.239244, 1764.239244, 1764.239244, 1764.239244, 1764.239244,
     #  1764.239244, 1764.239244, 1764.239244, 1764.239244, 1764.239244,
```

```
     #  1764.239244, 1764.239244, 1764.239244, 1764.239244, 1764.239244,
     #  1764.239244, 1764.239244, 1764.239244, 1764.239244, 1764.239244,
     #  1764.239244, 1764.239244, 1764.239244, 1764.239244, 1764.239244/
C
C* SPECIES SPECIFIC HEAT TABLES
C
      DATA (CPFTB(N, 1),N=1,50)
     #/ 9235.36,  9235.36,  9235.36,  9235.36, 9235.36,
     #  9235.36,  9235.36,  9235.36,  9235.36, 9235.36,
     #  9235.36,  9235.36,  9235.36,  9235.36, 9235.36,
     #  9235.36,  9235.36,  9235.36,  9235.36, 9235.36,
     #  9235.36,  9235.36,  9235.36,  9235.36, 9235.36,
     #  9235.36,  9235.36,  9235.36,  9235.36, 9235.36,
     #  9235.36,  9235.36,  9235.36,  9235.36, 9235.36,
     #  9235.36,  9235.36,  9235.36,  9235.36, 9235.36,
     #  9235.36,  9235.36,  9235.36,  9235.36, 9235.36,
     #  9235.36,  9235.36,  9235.36,  9235.36, 9235.36 /
C
      DATA (CPFTB(N, 2),N=1,50)
     #/ 1764.239244, 1764.239244, 1764.239244, 1764.239244, 1764.239244,
     #  1764.239244, 1764.239244, 1764.239244, 1764.239244, 1764.239244,
     #  1764.239244, 1764.239244, 1764.239244, 1764.239244, 1764.239244,
     #  1764.239244, 1764.239244, 1764.239244, 1764.239244, 1764.239244,
     #  1764.239244, 1764.239244, 1764.239244, 1764.239244, 1764.239244,
     #  1764.239244, 1764.239244, 1764.239244, 1764.239244, 1764.239244,
     #  1764.239244, 1764.239244, 1764.239244, 1764.239244, 1764.239244,
     #  1764.239244, 1764.239244, 1764.239244, 1764.239244, 1764.239244,
     #  1764.239244, 1764.239244, 1764.239244, 1764.239244, 1764.239244,
     #  1764.239244, 1764.239244, 1764.239244, 1764.239244, 1764.239244/
C
c23456789012345678901234567890123456789012345678901234567890123456789012
C
      DATA (CPFTB(N, 3),N=1,50)
     #/ 1764.239244, 1764.239244, 1764.239244, 1764.239244, 1764.239244,
     #  1764.239244, 1764.239244, 1764.239244, 1764.239244, 1764.239244,
     #  1764.239244, 1764.239244, 1764.239244, 1764.239244, 1764.239244,
     #  1764.239244, 1764.239244, 1764.239244, 1764.239244, 1764.239244,
     #  1764.239244, 1764.239244, 1764.239244, 1764.239244, 1764.239244,
     #  1764.239244, 1764.239244, 1764.239244, 1764.239244, 1764.239244,
     #  1764.239244, 1764.239244, 1764.239244, 1764.239244, 1764.239244,
     #  1764.239244, 1764.239244, 1764.239244, 1764.239244, 1764.239244,
     #  1764.239244, 1764.239244, 1764.239244, 1764.239244, 1764.239244,
     #  1764.239244, 1764.239244, 1764.239244, 1764.239244, 1764.239244/
C
C*******DATA FOR VIRIAL COEFFICIENTS***************
C********TEMPERATURE TABLE***********
      DATA (TTV(N),N=1,50)
     >/    0.0,    400.0,    800.0,   1200.0,   1600.0,
     >  2000.0,   2400.0,   2800.0,   3200.0,   3600.0,
     >  4000.0,   4400.0,   4800.0,   5200.0,   5600.0,
     >  6000.0,   6400.0,   6800.0,   7200.0,   7600.0,
     >  8000.0,   8400.0,   8800.0,   9200.0,   9600.0,
     > 10000.0, 10400.0, 10800.0, 11200.0, 11600.0,
     > 12000.0, 12400.0, 12800.0, 13200.0, 13600.0,
     > 14000.0, 14400.0, 14800.0, 15200.0, 15600.0,
     > 16000.0, 16500.0, 17500.0, 18500.0, 20000.0,
     > 30000.0, 50000.0, 70000.0, 90000.0,110000.0 /
C*********VIRIAL COEFFICIENT B********
      DATA (BVTB(N,  1),N=1,50)
     #/ 0.005125, 0.005125, 0.005125, 0.005125, 0.005125,
     #  0.005125, 0.005125, 0.005125, 0.005125, 0.005125,
     #  0.005125, 0.005125, 0.005125, 0.005125, 0.005125,
     #  0.005125, 0.005125, 0.005125, 0.005125, 0.005125,
     #  0.005125, 0.005125, 0.005125, 0.005125, 0.005125,
     #  0.005125, 0.005125, 0.005125, 0.005125, 0.005125,
     #  0.005125, 0.005125, 0.005125, 0.005125, 0.005125,
```

```
     #  0.005125, 0.005125, 0.005125, 0.005125, 0.005125,
     #  0.005125, 0.005125, 0.005125, 0.005125, 0.005125,
     #  0.005125, 0.005125, 0.005125, 0.005125, 0.005125 /
C
      DATA (BVTB(N,  2),N=1,50)
     #/ 0.02258961, 0.02258961, 0.02258961, 0.02258961, 0.02258961,
     #  0.02258961, 0.02258961, 0.02258961, 0.02258961, 0.02258961,
     #  0.02258961, 0.02258961, 0.02258961, 0.02258961, 0.02258961,
     #  0.02258961, 0.02258961, 0.02258961, 0.02258961, 0.02258961,
     #  0.02258961, 0.02258961, 0.02258961, 0.02258961, 0.02258961,
     #  0.02258961, 0.02258961, 0.02258961, 0.02258961, 0.02258961,
     #  0.02258961, 0.02258961, 0.02258961, 0.02258961, 0.02258961,
     #  0.02258961, 0.02258961, 0.02258961, 0.02258961, 0.02258961,
     #  0.02258961, 0.02258961, 0.02258961, 0.02258961, 0.02258961,
     #  0.02258961, 0.02258961, 0.02258961, 0.02258961, 0.02258961 /
C
      DATA (BVTB(N,  3),N=1,50)
     #/ 0.02258961, 0.02258961, 0.02258961, 0.02258961, 0.02258961,
     #  0.02258961, 0.02258961, 0.02258961, 0.02258961, 0.02258961,
     #  0.02258961, 0.02258961, 0.02258961, 0.02258961, 0.02258961,
     #  0.02258961, 0.02258961, 0.02258961, 0.02258961, 0.02258961,
     #  0.02258961, 0.02258961, 0.02258961, 0.02258961, 0.02258961,
     #  0.02258961, 0.02258961, 0.02258961, 0.02258961, 0.02258961,
     #  0.02258961, 0.02258961, 0.02258961, 0.02258961, 0.02258961,
     #  0.02258961, 0.02258961, 0.02258961, 0.02258961, 0.02258961,
     #  0.02258961, 0.02258961, 0.02258961, 0.02258961, 0.02258961,
     #  0.02258961, 0.02258961, 0.02258961, 0.02258961, 0.02258961 /
C
C*************VIRIAL COEFFICIENT C********
      DATA (CVTB(N,  1),N=1,50)
     >/ 0.00000,  0.00000,  0.00000,  0.00000,  0.00000,
     >  0.00000,  0.00000,  0.00000,  0.00000,  0.00000,
     >  0.00000,  0.00000,  0.00000,  0.00000,  0.00000,
     >  0.00000,  0.00000,  0.00000,  0.00000,  0.00000,
     >  0.00000,  0.00000,  0.00000,  0.00000,  0.00000,
     >  0.00000,  0.00000,  0.00000,  0.00000,  0.00000,
     >  0.00000,  0.00000,  0.00000,  0.00000,  0.00000,
     >  0.00000,  0.00000,  0.00000,  0.00000,  0.00000,
     >  0.00000,  0.00000,  0.00000,  0.00000,  0.00000,
     >  0.00000,  0.00000,  0.00000,  0.00000,  0.00000 /
C
      DATA (CVTB(N,  2),N=1,50)
     >/ 0.00000,  0.00000,  0.00000,  0.00000,  0.00000,
     >  0.00000,  0.00000,  0.00000,  0.00000,  0.00000,
     >  0.00000,  0.00000,  0.00000,  0.00000,  0.00000,
     >  0.00000,  0.00000,  0.00000,  0.00000,  0.00000,
     >  0.00000,  0.00000,  0.00000,  0.00000,  0.00000,
     >  0.00000,  0.00000,  0.00000,  0.00000,  0.00000,
     >  0.00000,  0.00000,  0.00000,  0.00000,  0.00000,
     >  0.00000,  0.00000,  0.00000,  0.00000,  0.00000,
     >  0.00000,  0.00000,  0.00000,  0.00000,  0.00000,
     >  0.00000,  0.00000,  0.00000,  0.00000,  0.00000 /
C*
      DATA (CVTB(N,  3),N=1,50)
     >/ 0.00000,  0.00000,  0.00000,  0.00000,  0.00000,
     >  0.00000,  0.00000,  0.00000,  0.00000,  0.00000,
     >  0.00000,  0.00000,  0.00000,  0.00000,  0.00000,
     >  0.00000,  0.00000,  0.00000,  0.00000,  0.00000,
     >  0.00000,  0.00000,  0.00000,  0.00000,  0.00000,
     >  0.00000,  0.00000,  0.00000,  0.00000,  0.00000,
     >  0.00000,  0.00000,  0.00000,  0.00000,  0.00000,
     >  0.00000,  0.00000,  0.00000,  0.00000,  0.00000,
     >  0.00000,  0.00000,  0.00000,  0.00000,  0.00000,
     >  0.00000,  0.00000,  0.00000,  0.00000,  0.00000 /
C*
C  TIME HISTORY FOR CURRENT IN MS
```

```
C*
C*
      DATA (CTIM(I),I=1,178)
     >/   0.000,    0.030,    0.060,    0.090,    0.120,
     >    0.150,    0.180,    0.210,    0.240,    0.270,
     >    0.300,    0.330,    0.360,    0.390,    0.420,
     >    0.450,    0.480,    0.510,    0.540,    0.570,
     >    0.600,    0.630,    0.660,    0.690,    0.720,
     >    0.750,    0.780,    0.810,    0.840,    0.870,
     >    0.900,    0.930,    0.960,    0.990,    1.020,
     >    1.050,    1.080,    1.110,    1.140,    1.170,
     >    1.200,    1.230,    1.260,    1.290,    1.320,
     >    1.350,    1.380,    1.410,    1.440,    1.470,
     >    1.500,    1.530,    1.560,    1.590,    1.620,
     >    1.650,    1.680,    1.710,    1.740,    1.770,
     >    1.800,    1.830,    1.860,    1.890,    1.920,
     >    1.950,    1.980,    2.010,    2.040,    2.070,
     >    2.100,    2.130,    2.160,    2.190,    2.220,
     >    2.250,    2.280,    2.310,    2.340,    2.370,
     >    2.400,    2.430,    2.460,    2.490,    2.520,
     >    2.550,    2.580,    2.610,    2.640,    2.670,
     >    2.700,    2.730,    2.760,    2.790,    2.820,
     >    2.850,    2.880,    2.910,    2.940,    2.970,
     >    3.000,    3.030,    3.060,    3.090,    3.120,
     >    3.150,    3.180,    3.210,    3.240,    3.270,
     >    3.300,    3.330,    3.360,    3.390,    3.420,
     >    3.450,    3.480,    3.510,    3.540,    3.570,
     >    3.600,    3.630,    3.660,    3.690,    3.720,
     >    3.750,    3.780,    3.810,    3.840,    3.870,
     >    3.900,    3.930,    3.960,    3.990,    4.020,
     >    4.050,    4.080,    4.110,    4.140,    4.170,
     >    4.200,    4.230,    4.260,    4.290,    4.320,
     >    4.350,    4.380,    4.410,    4.440,    4.470,
     >    4.500,    4.530,    4.560,    4.590,    4.620,
     >    4.650,    4.680,    4.710,    4.740,    4.770,
     >    4.800,    4.830,    4.860,    4.890,    4.920,
     >    4.950,    4.980,    5.010,    5.040,    5.070,
     >    5.100,    5.130,    5.160,    5.190,    5.220,
     >    5.250,    5.280,    5.310 /
C
C*  CURRENT HISTORY IN KA
C
      DATA (CURR(I),I=1,178)
     >/  0.1666,   1.1499,   1.5000,   3.4998,   5.4996,
     >   7.2772,   9.2771,   11.055,   12.610,   13.499,
     >   14.843,   16.398,   17.509,   18.842,   19.731,
     >   20.176,   21.953,   21.731,   22.175,   23.064,
     >   23.286,   23.286,   23.731,   24.175,   24.175,
     >   24.842,   24.175,   25.064,   25.064,   24.842,
     >   25.286,   25.508,   25.286,   25.953,   25.731,
     >   26.397,   27.064,   27.508,   28.175,   28.175,
     >   29.064,   29.952,   30.175,   31.508,   32.175,
     >   32.841,   33.286,   34.619,   35.063,   36.174,
     >   36.396,   37.730,   38.396,   39.285,   40.840,
     >   40.840,   41.951,   42.174,   43.285,   43.951,
     >   45.062,   44.840,   45.951,   46.173,   46.840,
     >   47.284,   47.729,   47.506,   48.173,   47.951,
     >   47.951,   48.840,   54.395,   61.283,   67.293,
     >   72.404,   77.514,   82.625,   86.847,   90.180,
     >   93.069,   96.179,   98.401,   99.957,   101.07,
     >   102.62,   103.29,   104.40,   104.85,   105.29,
     >   105.96,   107.07,   107.07,   108.18,   109.29,
     >   110.40,   111.73,   112.84,   114.63,   116.41,
     >   118.19,   119.97,   121.52,   123.97,   125.52,
     >   127.08,   128.41,   130.19,   131.74,   132.63,
     >   133.52,   134.63,   135.74,   136.63,   136.63,
```

```
>   136.41,   136.19,   135.08,   133.74,   133.08,
>   132.41,   130.85,   129.52,   127.52,   125.52,
>   123.30,   121.30,   119.30,   116.63,   113.97,
>   111.29,   107.29,   104.62,   101.51,   98.624,
>   94.180,   90.847,   86.625,   83.069,   78.848,
>   75.959,   72.404,   69.515,   65.960,   63.283,
>   60.394,   57.506,   55.061,   52.617,   49.951,
>   48.173,   46.840,   44.396,   43.062,   41.063,
>   39.507,   37.730,   35.952,   34.619,   32.619,
>   30.841,   29.286,   27.730,   26.175,   24.397,
>   22.175,   20.176,   18.176,   17.065,   14.843,
>   13.499,   11.721,   10.388,    8.833,    7.277,
>    5.722,    4.389,    3.278 /
  END
```

INTENTIONALLY LEFT BLANK.

NO. OF COPIES	ORGANIZATION
2	DEFENSE TECHNICAL INFO CTR ATTN DTIC DDA 8725 JOHN J KINGMAN RD STE 0944 FT BELVOIR VA 22060-6218
1	DIRECTOR US ARMY RESEARCH LAB ATTN AMSRL OP SD TA 2800 POWDER MILL RD ADELPHI MD 20783-1145
3	DIRECTOR US ARMY RESEARCH LAB ATTN AMSRL OP SD TL 2800 POWDER MILL RD ADELPHI MD 20783-1145
1	DIRECTOR US ARMY RESEARCH LAB ATTN AMSRL OP SD TP 2800 POWDER MILL RD ADELPHI MD 20783-1145
	ABERDEEN PROVING GROUND
5	DIR USARL ATTN AMSRL OP AP L (305)

NO. OF COPIES	ORGANIZATION
1	DIRECTOR BENET LABORATORIES ATTN W KITCHENS USA WATERVLIET ARSENAL WATERVLIET NY 12189
1	COMMANDER USA ARDEC ATTN SMCAR FSA T M SALSBURY PICATINNY ARSENAL NJ 07806-5000
1	COMMANDER USA ARDEC ATTN SMCAR FSE T GORA PICATINNY ARSENAL NJ 07806-5000
2	COMMANDER USA RSRSCH OFC ATTN TECH LIB D MANN PO BOX 12211 RESEARCH TRIANGLE PK NC 27709-2211
1	PRESIDENT USA ARTILLERY BOARD FT SILL OK 73503
1	COMMANDANT USA CMD & GEN STAFF COLL FT LEAVENWORTH KS 66027-5200
1	COMMANDANT USA SPECIAL WARF SCHL ATTN REV & TNG LIT DIV FT BRAGG NC 28307
1	COMMANDER RADFORD ARMY AMMUN PLANT ATTN SMCRA QA HI LIBRARY RADFORD VA 24141
1	COMMANDANT USA FLD ART SCHL ATTN STSF TSM CN FT SILL OK 73503-5600
1	NAVAL RESEARCH LAB TECHNICAL LIBRARY WASHINGTON DC 20375

NO. OF COPIES	ORGANIZATION
3	COMMANDER NSWC ATTN 610 C SMITH 6110J K RICE 6110C S PETERS INDIAN HEAD MD 20640-5035
2	COMMANDER ATTN CODE G33 T DORAN J COPLEY DAHLGREN VA 22448-5000
1	PENN STATE UNIV DEPT OF MECH ENGR ATTN DR K KUO 312 MECH ENG BLDG UNIVERSITY PK PA 16802
1	NC STATE UNIV ATTN J G GILLIGAN BOX 7909 1110 BURLINGTON ENG LABS RALEIGH NC 27695-7909
3	INST FOR ADV STUDIES ATTN DR H FAIR DR T KIEHNE DR I MCNAB 4030 2 W BAKER LN AUSTIN TX 78759-5329
3	FMC CORPORATION ATTN B GODDELL DR D COOK J DYVIK 4800 E RIVER RD MINNEAPOLIS MN 55421-1498
1	ALLIANT TECHSYSTEMS INC ATTN J KENNEDY MN38 3300 10400 YELLOW CIRCLE DR MINNETONKA MN 55343
1	PAUL GOUGH ASSOCIATES INC ATTN P S GOUGH 1048 SOUTH ST PORTSMOUTH NH 03801-5423

NO. OF COPIES	ORGANIZATION
1	PRINCETON COMB RSRCH LAB PRINCETON CORP PLAZA ATTN N MESSINA 11 DEERPARK DR BLDG IV STE 119 MONMOUTH JUNCTION NJ 08852
1	ELI FREEDMAN & ASSOC ATTN E FREEDMAN 2411 DIANA RD BALTIMORE MD 21209
1	VERITAY TECHNOLOGY INC 4845 MILLERSPORT HWY PO BOX 305 EAST AMHERST NY 14051-0305
1	GENERAL ELECTRIC CO DEFENSE SYS DIV ATTN DR J MANDZY MAIL DROP 43 220 100 PLASTICS AVE PITTSFIELD MA 01201
1	STATE UNIV OF NY DEPT OF ELECT ENGRG ATTN DR W J SARGEANT BONNER HALL RM 312 BUFFALO NY 14260
1	USA RSRCH OFC ENGINEERING SCI DIV ATTN DR D MANN 4300 S MIAMI BLVD RESEARCH TRIANGLE PARK NC 27709
1	ARMY HIGH PERFORM CMPTG RSRCH CTR UNIV OF MINNESOTA ATTN DR T TEZDUYAR 1100 WASHINGTON AVE S STE 101 MINNEAPOLIS MN 55415
3	COMBUSTION RSRCH & FLOW TECH INC ATTN DR A HOSANGADI 174 N MAIN ST BLDG 3 PO BOX 1150 DUBLIN PA 18917

NO. OF COPIES	ORGANIZATION
	ABERDEEN PROVING GROUND
22	DIR, USARL ATTN: AMSRL-WT-PA, T. MINOR G. WREN (2 CPS) W. OBERLE P. TRAN J. DESPIRITO T. COFFEE M. NUSCA G. KELLER D. KOOKER J. KNAPTON R. ANDERSON G. KATULKA K. WHITE P. CONROY S. RAY AMSRL-WT-PB, P. PLOSTINS AMSRL-WT-PC, R. FIFER AMSRL-WT-PD, B. BURNS AMSRL-WT-WD, J. POWELL AMSRL-WT-WG, P. KASTE E. SCHMIDT

NO. OF COPIES	ORGANIZATION
2	RARDE ATTN DR C WOODLEY MR STEVE GILBERT GS2 DIVISION BULDING R31 FORT HALSTEAD SEVENOAKS KENT TN14 7BP ENGLAND
5	WEAPONS SYSTEM DIVISION ATTN DR ANNA WILDEGGER-GAISSMAIER PO BOX 1500 SALISBURY, SOUTH AUSTRALIA 5108

USER EVALUATION SHEET/CHANGE OF ADDRESS

This Laboratory undertakes a continuing effort to improve the quality of the reports it publishes. Your comments/answers to the items/questions below will aid us in our efforts.

1. ARL Report Number ARL-TR-994 Date of Report April 1996

2. Date Report Received _____

3. Does this report satisfy a need? (Comment on purpose, related project, or other area of interest for which the report will be used.) _____

4. Specifically, how is the report being used? (Information source, design data, procedure, source of ideas, etc.) _____

5. Has the information in this report led to any quantitative savings as far as man-hours or dollars saved, operating costs avoided, or efficiencies achieved, etc? If so, please elaborate. _____

6. General Comments. What do you think should be changed to improve future reports? (Indicate changes to organization, technical content, format, etc.) _____

CURRENT ADDRESS

_____
Organization

_____
Name

_____
Street or P.O. Box No.

_____
City, State, Zip Code

7. If indicating a Change of Address or Address Correction, please provide the Current or Correct address above and the Old or Incorrect address below.

OLD ADDRESS

_____
Organization

_____
Name

_____
Street or P.O. Box No.

_____
City, State, Zip Code

(Remove this sheet, fold as indicated, tape closed, and mail.)

(DO NOT STAPLE)